VIBRATION-BASED ALGORITHM FOR DIAGNOSTIC AND PROGNOSTIC CONDITION MONITORING OF RAILROAD BEARINGS AND WHEELS

A Thesis

by

JEFFERY R. PAMS

Submitted in Partial Fulfillment of the

Requirements for the Degree of

MASTER OF SCIENCE IN ENGINEERING

Major Subject: Mechanical Engineering

The University of Texas Rio Grande Valley

May 2025

VIBRATION-BASED ALGORITHM FOR DIAGNOSTIC AND PROGNOSTIC CONDITION MONITORING OF RAILROAD BEARINGS AND WHEELS

A Thesis

by

JEFFERY R. PAMS

COMMITTEE MEMBERS

Dr. Constantine Tarawneh

Chair of Committee

Dr. Arturo Fuentes

Committee Member

Dr. Heinrich Foltz

Committee Member

May 2025

Copyright © 2025 Jeffery R. Pams
All Rights

ABSTRACT

Pams, Jeffery R., Vibration-Based Algorithm for Diagnostic and Prognostic Condition Monitoring of Railroad Bearings and Wheels. Master of Science in Engineering (MSE), May 2025, 60 pp., 5 tables, 38 figures, 24 references.

Bearing and wheel failure accounts for the majority of equipment-related train derailments on US railroads. Current wayside monitoring systems have been insufficient in the prevention of catastrophic derailments prompting the rail industry to explore the possible integration of onboard condition monitoring systems into their rail operations. The University Transportation Center for Railway Safety (UTCRS) in partnership with Hum Industrial Technology, Inc., has developed a wireless onboard system intended for the condition monitoring of railroad bearings and wheels. This thesis presents the development, evaluation, and implementation of an algorithm designed to be used in conjunction with these systems to provide railroad operators with diagnostic and prognostic estimates. Laboratory testing and field implementation results demonstrate the potential of this algorithm to accurately identify and diagnose defective bearings and wheels and provide remaining useful life estimates for bearings. This information can aid the rail industry in scheduling proactive maintenance cycles and mitigating unnecessary and expensive train stoppages.

DEDICATION

This thesis is dedicated to my mother, Jessica, for always supporting me and motivating me to pursue my educational goals. I also dedicate it to my little brothers, Jonathan and Joshua, whom I hope to inspire to dream big and pursue and achieve their goals in life.

ACKNOWLEDGEMENTS

Firstly, I would like to express my gratitude and appreciation to all my peers and faculty from the Railway Safety team. To Dr. Heinrich Foltz and the electrical team, your assistance and guidance in electrical matters was indispensable to my research. To the machinists, especially Daniel, your skills were immensely beneficial to the success of this project and for that I am grateful. To the rest of my teammates, Santana, Abel, Curtis, Diego, Eddie, Aaron, David, Roger, and everyone else, thank you for making my time here some of the best years of my life. We have persevered through thick and thin, and the laughs and memories we have shared will stay with me until the day I die. Each and every one of you has the potential to achieve greatness, and I know you all will be incredibly successful in your future endeavors.

This research was made possible through a partnership with Hum Industrial Technology, Inc., who provided financial and logistical support for the project. The work was also financially supported by the University Transportation Center for Railway Safety through the USDOT UTC Program under Grant No. 69A3552348340.

Finally, I want to express my utmost and sincere gratitude to the one and only Dr. Constantine Tarawneh. Thank you for giving me the opportunity to be a part of this excellent center that your hard work and dedication has built over the years. None of this would have been possible without your guidance. Your wisdom and mentorship have undoubtedly shaped me into who I am today, and for that I am eternally grateful

TABLE OF CONTENTS

Page

LIST OF TABLES

Page

LIST OF FIGURES

Page

CHAPTER I

BACKGROUND AND INTRODUCTION

1.1 Railway Tapered-Roller Bearings

Double-row tapered-roller bearings are utilized in the railway industry to support the heavy loads associated with freight rail transport. The railcar load is transmitted into the bearing to allow the axle and wheels to freely rotate as the car travels forward. The load is distributed evenly amongst eight bearings on each railcar that are mounted to the ends of the wheel-axle assemblies as depicted in Figure 1. The Association of American Railroads (AAR) classifies bearings based on their dimensions and load capacity. Table 1 summarizes the measurements and load rating for commonly used bearing classes in North America.

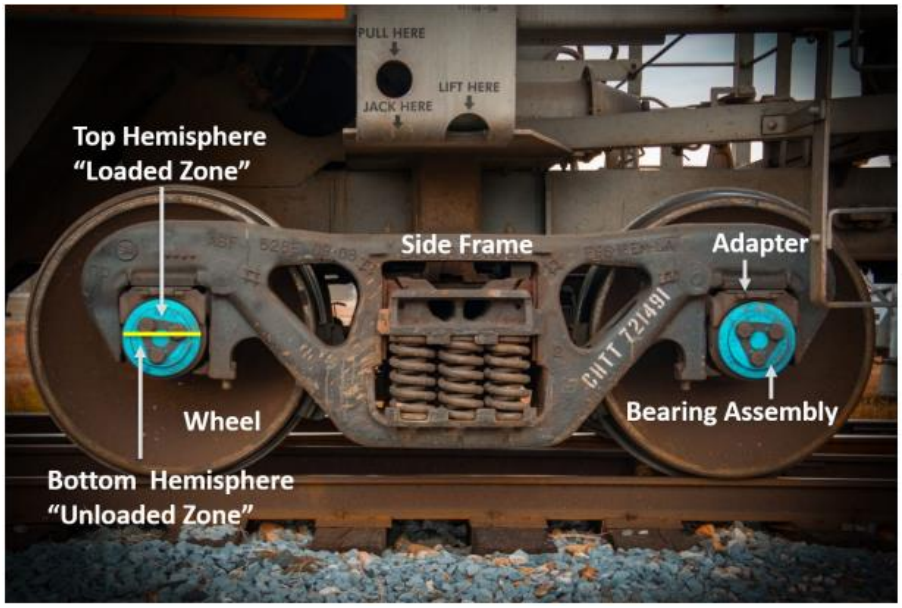

Figure 1: Side profile of railcar bogie assembly [1]

Table 1: AAR bearing class dimensions and load ratings [2]

Bearing Class	Cup Dimension Diameter × Width [inch]	Bearing Load [kN] / [kips]
E	6 × 11	117.0/26.3
F	6 ½ × 12	153.0/34.4
G	7 × 12	169.0/38.0
K	6 ½ × 9	153.0/34.4

1.1.1 Bearing Components and Operation

Figure 2 displays the components of a freight railcar tapered-roller bearing assembly. These components include the outer ring (cup), two inner ring (cone) assemblies, the spacer ring, two grease seals, and two wear rings. The cone assembly is further subdivided into the cage, tapered rollers, and the cone itself.

Under normal operation, the bearing cup, which houses the cone assemblies, remains stationary under the load of the railcar via the side frame and the bearing adapter. However, improper tolerances, worn components, and shock loading can lead to a phenomenon known as “indexing” where the cup slowly rotates under the adapter housing. The two cone assemblies are mounted to the axle assembly via an interference fit. The cone assemblies are separated by the spacer ring which accommodates a preset amount of lateral movement (up to 0.028") that can occur during sharp turns or bogie hunting events. The cage acts as a separator that evenly spaces the rollers along the raceways. The grease seals serve to prevent lubricant leakage and mitigate contamination, which degrades lubrication quality and decreases bearing life.

Figure 2: Components of a railway tapered-roller bearing [2]

The bearing aims to serve as a mechanically efficient way to support the load of the railcar while allowing the axle to rotate with minimal friction. It accomplishes this by taking advantage of the lower friction provided by rolling contact coupled with elastohydrodynamic lubrication. Axle and wheel rotation causes the cones to rotate concurrently, which causes the rollers to rotate and revolve about the cup and cone raceways. This motion causes the grease to circulate and create a lubrication film between the rollers and raceways. Proper assembly and lubrication are crucial to the efficient and reliable operation of these bearings.

1.1.2 Bearing Defects

Despite the lower friction and suppressed wear afforded by these bearings, they remain susceptible to significant damage, primarily due to rolling contact fatigue (RCF). RCF occurs due to the Hertzian contact stresses between the rollers and raceways that are applied cyclically as the bearing rotates. The resulting damage is especially exacerbated by the presence of subsurface inclusions (impurities in the bearing material) in the region of maximum subsurface shear stress. These defects below the raceway surfaces act as stress concentrations that can be

severely detrimental to the bearing service life. After many cycles, microcracks can initiate at these inclusions and propagate to the surface, forming small pits. This leads to spalling, a phenomenon where flakes of metal break away from the surface. The aforementioned typically occurs on the raceways of the bearing rings and on the rollers. Figure 3 displays an example of spalling and pitting damage on a bearing cone.

Lubricant contamination is also a leading cause of bearing damage and subsequent failure. Faulty seals can allow contaminants, such as dirt or water, to enter the grease and degrade its lubricating ability. This leads to accelerated wear on the bearing components and decreases service life. Water contamination is especially common in field service. Water reacts with the grease and corrodes the raceway surface in patterns corresponding to the spacing of the rollers. This phenomenon, known as water-etching, creates etch marks that severely weaken the raceway material, which allows the damage to propagate as the bearing continues operating. An example of water-etch damage can be observed in Figure 4.

Figure 3: Fatigue spalling and pitting on a cone raceway [2]

Figure 4: Water-etch damage on a cone raceway [2]

Regardless of mechanism, damage to the bearing raceways and rolling elements can be dangerous and lead to catastrophic failure. This is because defects compromise the smooth rolling contact between the rollers and raceways, which can lead to roller misalignments. If left unchecked, the damaged areas could become extensive enough to trigger severe roller misalignments, leading to the rollers sliding across the raceway or even bearing seizure. This causes rapid overheating from increased friction, eventually resulting in the bearing “twisting off” the axle and causing a catastrophic derailment.

1.2 Rolling Stock Wheels

Railway transportation is regarded as the most efficient land-based method of transporting goods and passengers. This is due to the relatively low friction between the steel-on-steel interactions between the wheels and rails as opposed to the rubber-on-pavement interactions between automobile tires and pavement. This leads to higher fuel efficiency and enables higher

freight loads to be transported at a fraction of the cost. Freight railcars are equipped with four wheel-axle assemblies (also known as wheelsets), each containing two semi-conical wheels mounted on a single axle via an interference fit.

1.2.1 Wheel Components and Operation

Railcar wheels are designed in such a way to ensure that the train remains on the track during operation. The components of a wheelset include the axle, two wheels, and two tapered-roller bearings mounted on the ends of the axle. The wheels themselves are subdivided into the wheel tread, wheel flange, wheel hub, wheel bore, wheel web, and the front and back face rims. A diagram labelling the wheel components is depicted in Figure 5.

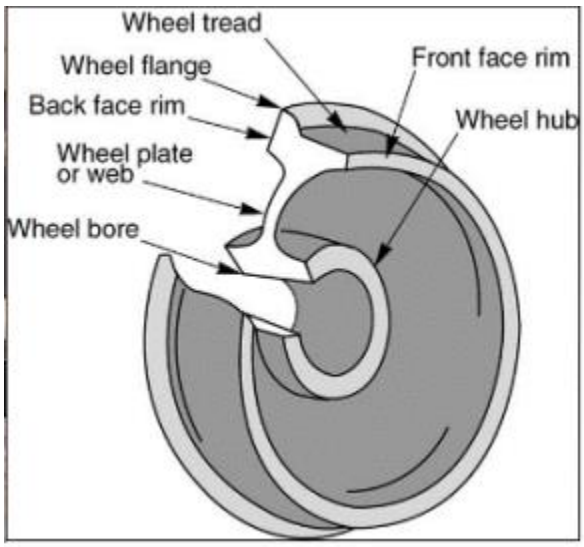

Figure 5: Diagram of railcar wheel [3]

Since the wheels are mounted rigidly to the axle, they rotate at the same speed regardless of track geometry. This can be problematic on curves as one wheel will have to travel a longer distance than the other. The semi-conical shape of the wheel tread compensates for this difference. This geometry behaves similarly to a differential gearbox in automobiles, which

enables the wheels to rotate at different speeds, thus ensuring the train can navigate the curve safely without derailing. The wheel flange also contributes by providing a barrier that prevents the wheel from slipping off the rail during turning maneuvers.

1.2.2 Wheel Defects

Railcar wheels are especially prone to defects due to the demanding conditions they experience in field service. These defects can be categorized into three main categories: visually evident, geometric, and subsurface defects. Visually evident defects include wheel flats, shelling, and thermal cracks, with examples depicted in Figure 6. Wheel flats occur as a result of localized wear on the wheel tread due to sliding friction typically from braking. Shelling, like spalling in bearing raceways, is characterized by the flaking of metal fragments from the wheel surface as a result of surface RCF. Thermal cracks originate from fatigue induced by thermal stresses experienced in operation.

Figure 6: Wheel flat (left) and wheel tread shelling (right)

Geometric defects typically cannot be identified by the naked eye and require gauges to validate. These include thin flanges, hollow flanges, deep flanges, hollow treads, etc. A representation of a hollow tread can be seen in Figure 7, along with the gauge used to identify it. These defects typically arise as a result of wear between the wheel and rail surfaces. Subsurface defects include subsurface porosity and internal cracks which can only be identified with special techniques such as ultrasonic scanning.

Regardless of origin, wheel defects are highly detrimental to the structural integrity of the wheel and the rail infrastructure that it interacts with. These defects generate high impact forces and high-frequency vibrations that can severely damage the wheel and track and lead to catastrophic failure if not acted upon in a timely manner.

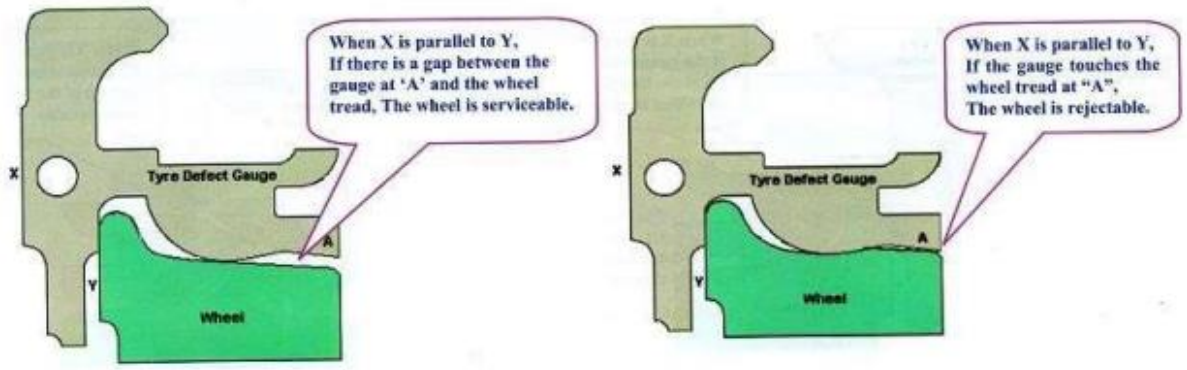

Figure 7: Hollow tread [4]

1.3 Wayside Condition Monitoring Systems

According to statistics published by the Federal Railroad Administration (FRA), defective bearings and wheels were among the leading causes of train derailments in the United States in 2024 [5], which necessitates the monitoring of these mechanical components to mitigate

the risk of catastrophic failure. The railway industry currently employs wayside detection systems to monitor defective bearings and wheels. These systems are integrated into the track infrastructure and alert railway operators when these components exhibit abnormal behavior that requires remediation. For bearings, these systems include Hot Bearing (or Box) Detectors (HBDs) and Trackside Acoustic Detection Systems (TADS™). For wheels, Wheel Impact Load Detectors (WILDs) are utilized.

1.3.1 Hot Bearing Detectors (HBDs)

Hot Bearing Detectors, pictured in Figure 8, utilize infrared sensors to measure the temperature radiating from bearings in operation. According to standards set by the Association of American Railroads (AAR), HBDs will alert train operators if a bearing is operating at a temperature higher than 94.4°C (170°F) above ambient or higher than 52.8°C (95°F) above the temperature of the mate bearing on the opposite side of the axle [6].

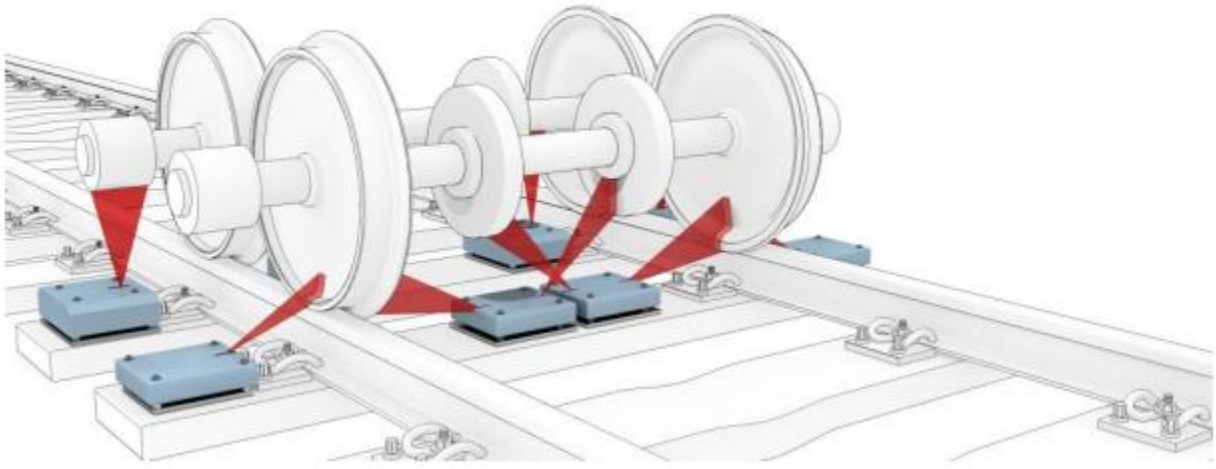

Figure 8: Illustration of a Hot Bearing Detector site [9]

Over 6,000 HBDs are installed across US railways with spacing ranging from 24 to 48 km (15 to 30 mi) apart [7]. In response to the 2023 catastrophic derailment in East Palestine, Ohio, that was caused by an overheated bearing that an HBD flagged minutes before the incident, the industry began to install approximately 1,000 new HBDs across key routes that mitigated gaps in the system [8]. Despite these efforts, derailments resulting from overheating bearings highlight the limitations of relying solely on these systems. In addition to inadequate spacing, reliance on temperature as a metric for condition monitoring may not be adequate for the timely and proactive detection of defective bearings. Studies have shown that defective bearings can operate at temperatures well below the AAR-established threshold [10, 11]. Defective bearings typically do not exhibit thermal indications of distress until catastrophic failure is imminent. This was exemplified by the East Palestine derailment where the overheating bearing caused the train to derail within minutes of being flagged [12].

1.3.2 Trackside Acoustic Detection Systems (TADS™)

Trackside Acoustic Detection Systems, pictured in Figure 9, employ microphones to detect the acoustic emissions of bearings in operation. Bearing defects generate elevated vibrations that are transmitted through the air as acoustic signals that can be detected by the TADS™. These systems are effective in detecting bearings that are nearing the end of their service life. However, these systems are rare along North American railways, meaning a bearing can spend its entire service life without passing through a TADS™ site [14]. Moreover, their current configuration/thresholds have shown to not be proficient in identifying bearings with defects on the inboard raceways (closest to the railcar) [15] without increasing the false positive

rate.

Figure 9: TADS™ site [13]

1.3.3 Wheel Impact Load Detectors (WILDs)

The most common wayside detectors for wheel monitoring are Wheel Impact Load Detectors, an example of which can be seen in Figure 10. These systems consist of strain gauges mounted to the track that are designed to measure the forces generated by wheel-rail interactions. Table 2 summarizes the AAR standards regarding WILD measurements and the corresponding recommended maintenance practices.

Figure 10: WILD site [16]

Table 2: AAR guidelines for WILD measurements [16]

Impact Force [kip]	Impact Force [kN]	Contemporary Recommended Practices
65-79	290-351	Owner can choose to shop car for repair
80-89	356-396	If car is shopped for non-wheel repairs, then repair facility is allowed to conduct wheel related repairs as well
90-139	400-618	Operating railroad is required to shop car upon arrival to destination
140+	623+	Operating railroad is required to inspect train and move it at speeds under 48 km/h (30 mph) to set out affected car

According to the Transportation Technology Center, Inc. (now known as MxV Rail), a subsidiary of the AAR, there were 191 active WILD systems in use as of 2020 [17]. While more may have been installed in the years since, the low amount and dispersion of these systems across hundreds of thousands of miles of rail in the US highlights the challenge of continuous monitoring of wheel conditions. Defective wheels can deteriorate rapidly which could lead to

catastrophic failure even if they are flagged by a WILD measurement. This was the case in the 2018 derailment of a Canadian National (CN) Railway Company freight train that was caused by a shattered rim on one of its wheels [18]. The defective wheel had passed through multiple WILD sites in the month leading up to the derailment with readings reaching up to 485kN (109 kip) on the day the train ultimately derailed. As per AAR standards, these readings require operators to conduct maintenance upon arrival to the next destination. However, the fact that catastrophic failure occurred before the train was able to reach its destination underscores that these WILD systems and the standards associated with them are not always sufficient in preventing wheel-related derailments.

1.4 Onboard Condition Monitoring

Due to the limitations inherent in wayside condition monitoring systems, efforts are being made to transition to alternative methods that enable the continuous monitoring of bearings and wheels. These systems have the potential to close the gaps in the current condition monitoring infrastructure and aid in the timely notification of defective components.

1.4.1 Vibration Monitoring

Vibration analysis is used as a condition monitoring technique to determine the health of machinery in a wide variety of industries. Researchers at the University Transportation Center for Railway Safety (UTCRS) at the University of Texas-Rio Grande Valley (UTRGV) have been working for the past two decades to apply vibration-based condition monitoring to the railway industry. The UTCRS algorithm, developed by Alvarado [19] and further optimized by Gonzalez [20] and Montalvo [21], has proved to be effective in identifying defective bearings, determining which component is defective, and estimating the approximate size of the defect in both laboratory experiments and field tests.

1.4.2 Wireless Vibration Monitoring System

In order to facilitate the implementation of vibration-based monitoring into field service, the UTCRS, in partnership with Hum Industrial Technology, Inc., has developed a wireless onboard condition monitoring sensor module known as the “Boomerang”. This module hosts a suite of sensors that are capable of measuring bearing operating temperature and the vibrations emitted from bearings and wheel-rail interactions. Studies conducted by Cantu [22] and Barrera [23] have demonstrated the capabilities of the Boomerang in the continuous condition monitoring of bearings and wheels.

1.4.3 Challenges and Motivation

Despite the potential of onboard condition monitoring systems, the development and field implementation of the Hum Boomerang has been met with some challenges inherent in the nature of field condition monitoring. One such challenge is the power required for the continuous operation of these wireless devices in field service. Research is ongoing to explore energy harvesting solutions, such as solar cells, and optimizations to the operation firmware of the device to reduce its power requirements. This will extend the service life of the Boomerang to the desired 10+ years of operation (currently at 5-6 years). Other challenges include optimizing the algorithm to accurately differentiate between defective bearings and wheels in the noisy field service operating conditions that introduce variability into the data, making diagnostics and prognostics a bit more challenging.

Hence, the goal of the work presented in this thesis is to develop an optimized algorithm that can address the data-related challenges to enhance the ability of the Boomerang to accurately provide diagnostics and prognostics for railway bearings and wheels. Chapter II details the laboratory and field setups and methodologies utilized to collect the data used for this study.

Chapter III introduces the Bearing Health Index (BHI) and Wheel Health Index (WHI) and their implementation for the provision of diagnostics and prognostics. Chapter IV details the methods used to account for variability in the data collected from the field. Chapter V presents the complete field monitoring algorithm. Chapter VI evaluates the efficacy of the algorithm in the laboratory and in the field. Conclusions, limitations, and future work proposals are discussed in Chapter VII.

CHAPTER II

EXPERIMENTAL SETUPS

2.1 Laboratory Setups

To develop the correlations used in this thesis, data was collected from two decades worth of bearing experiments conducted at the UTCRS facilities. These experiments were conducted using specially designed dynamic test rigs that mimic railway bearing operation in field service. These include four-bearing test rigs (4BT) and a single-bearing test rig (SBT).

2.1.1 Four-Bearing Test Rig

Currently, the UTCRS laboratories house four Four-Bearing Testers (4BT). These test rigs have the capacity to test four bearings mounted on a custom test axle simultaneously. They can accommodate AAR class E, F, G, and K bearings with the two newest rigs also able to accommodate AAR class GG bearings. The bearings are mounted to the custom test axle via a 300-ton hydraulic press and placed on the test rigs as can be seen in Figure 11. The outer bearings are supported on the tester table by railcar adapters while the inner bearings are top-loaded with adapters and an I-beam to distribute the load. Since top-loading is the more realistic representation of field conditions, data for this thesis was taken solely from the middle two bearings in experiments conducted with the 4BTs.

The testers are equipped with hydraulic cylinders capable of applying loads up to 150% of the AAR rated bearing loads (see Table 1). The applied load is regulated by specially designed

load controller systems that monitor the load and adjust the pressure of the hydraulic cylinder as necessary to maintain a constant load throughout testing. The drivetrain for each tester consists of a 22 kW (30 hp) variable-speed electric motor controlled by a Variable Frequency Drive (VFD) and a pulley-belt system that transmits the rotation of the motor to the axle. This system enables the simulation of train speeds up to 137 km/h (85 mph). The bearings are cooled in operation by two blowers that can provide a variable speed airflow ranging from 1 to 36 m/s (~2-80 mph).

Figure 11: Four-Bearing Tester (4BT)

2.1.2 Single-Bearing Test Rig

The UTCRS facilities currently possess one Single-Bearing Tester (SBT) that is shown in Figure 12. This tester was designed to closely mimic the way bearings are mounted in field service as well as simulate lateral and impact loads. The SBT can only test one bearing (Class E, F, G, or K) at a time with the bearing being mounted to the test axle by a specially designed portable hydraulic press. The test axle is supported by two spherical-roller pillow block bearings while the test bearing is mounted and loaded in a cantilever fashion. This cantilever setup is the most realistic simulation of bearings under load in the field. The SBT is also equipped with an impact mechanism that can simulate the impact forces generated by the wheel-rail interactions of defective wheels and tracks. It also comes equipped with a lateral loading system that can simulate the lateral forces generated as trains navigate curved sections of tracks.

2.1.3 Instrumentation and Data Acquisition

The vibration data used in this study was measured utilizing a uniaxial microelectromechanical system (MEMS) accelerometer with a measuring range of 100 g. These accelerometers are mounted to specially machined railway adapters as seen in Figure 13. Data was collected for 16 seconds every 10 minutes over the duration of an experiment. NI cDAQ-9174 chassis, NI 9215 and NI 9239 DAQ modules, and NI LabVIEW were used to collect data from the accelerometers. Temperature, load, and motor power were also recorded using K-Type thermocouples, load cells, and the VFD outputs, respectively. These measurements helped monitor the bearing and tester condition for abnormalities. However, the data from these measurements was not pertinent for this thesis.

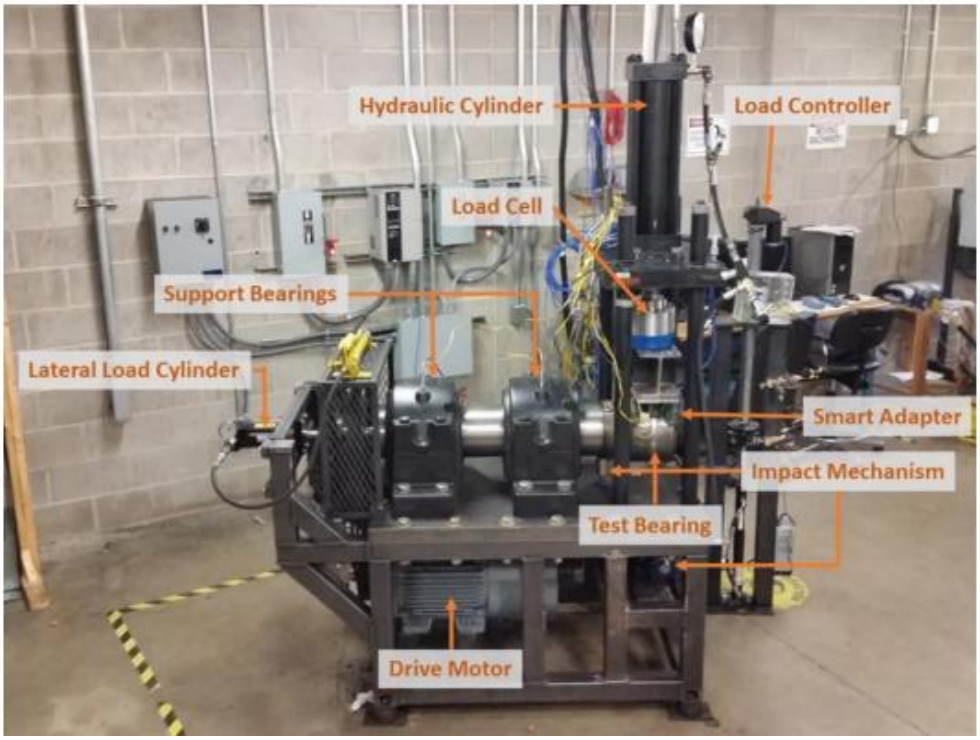

Figure 12: Single-Bearing Tester (SBT)

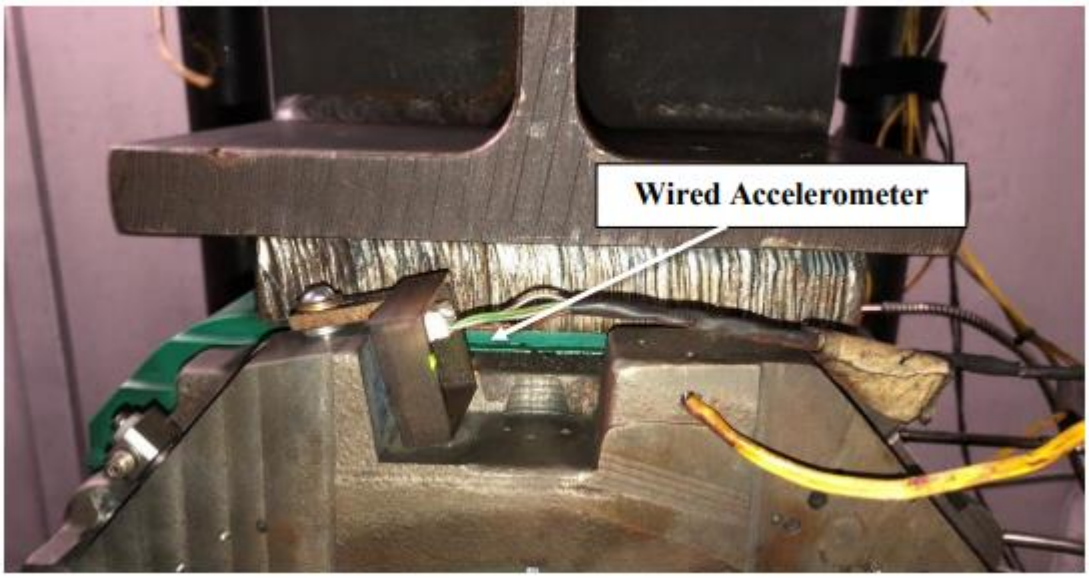

Figure 13: Accelerometer placement

2.2 Field Test Setup

To evaluate the performance of the Boomerang in field conditions, multiple pilot tests were conducted over the past four years on freight rail lines. This section summarizes the hardware and installation procedures utilized to conduct these tests.

2.2.1 Hum Boomerang

The Hum Boomerang, in its current configuration, is a battery-powered wireless module designed for continuous condition monitoring of rolling stock. It hosts a suite of sensors that measure the vibration and operating temperatures. To measure vibration, the Boomerang is equipped with two accelerometers denoted as A1 and A2. A1 is a single-axis accelerometer with a ±100 g measuring range. It is coupled with an analog low-pass filter to filter out high-frequency vibrations, which are characteristic of impacts from defective wheels and track. This setup is designed for optimal bearing condition monitoring. A2 is a tri-axial accelerometer with a ±200 g measuring range. This accelerometer was incorporated for the purpose of wheel impact detection. It should be noted that the Boomerang version used for the field tests discussed in this thesis was V5, or the fifth iteration. The V6 is the current version of the Boomerang that is still undergoing research and development for the integration of load sensing capabilities.

2.2.2 Hum Gateway

The Hum Gateway is a solar-powered wireless communication module that receives data measured by the Boomerangs and transmits it via cellular data transmission to Hum's online dashboard. It is also used to flash the Boomerangs with firmware updates and modify parameters such as sampling rate, recording intervals, etc. The Gateway is also capable of providing the GPS

location of data points and utilizes GPS to determine speed and loading conditions (fully loaded or empty).

2.2.3 Installation Procedures

The Boomerangs are designed to be mounted to the railcar bearing adapters to optimize the capture of vibration data from bearings and wheels in field service. The adapters are machined utilizing drill and tap methods to facilitate the mounting of the Boomerang case with steel screws as shown in Figure 14. Eight Boomerangs are installed per railcar and are designated by their position as per AAR nomenclature (Figure 15). For instance, the left wheel/bearing on the frontmost axle would be designated as L4. The eight Boomerangs are assigned to a single Gateway that is mounted in a strategic location on the railcar to optimize sunlight exposure (Figure 16).

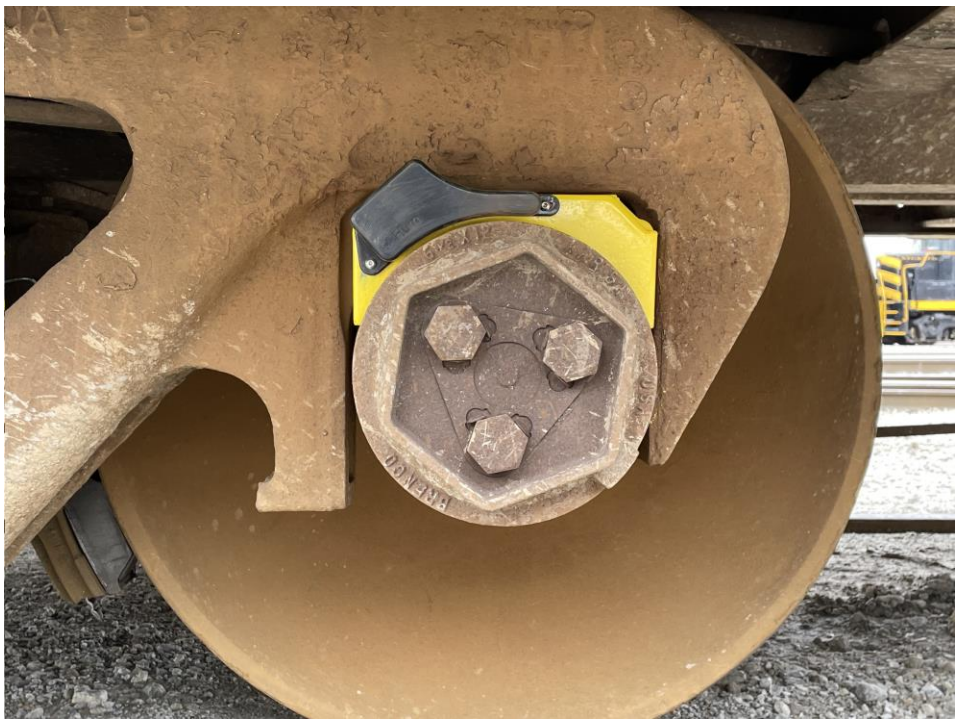

Figure 14: V5 Boomerang mounted on railcar bearing adapter

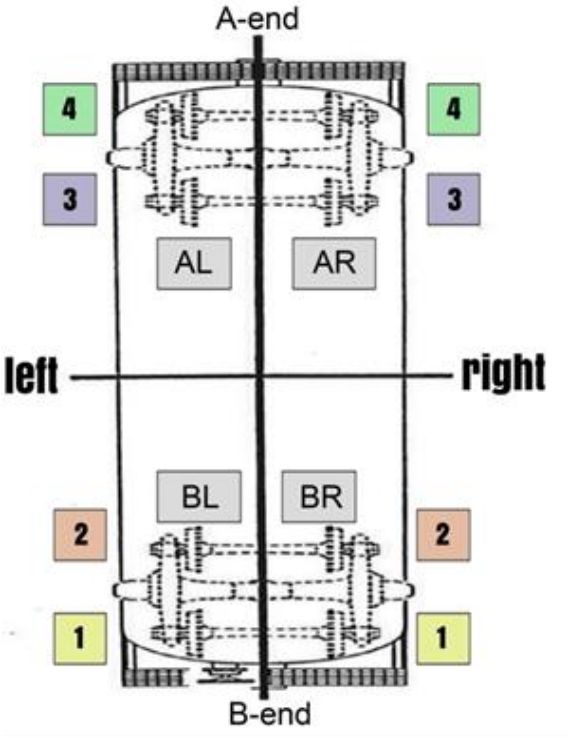

Figure 15: AAR wheel identification diagram

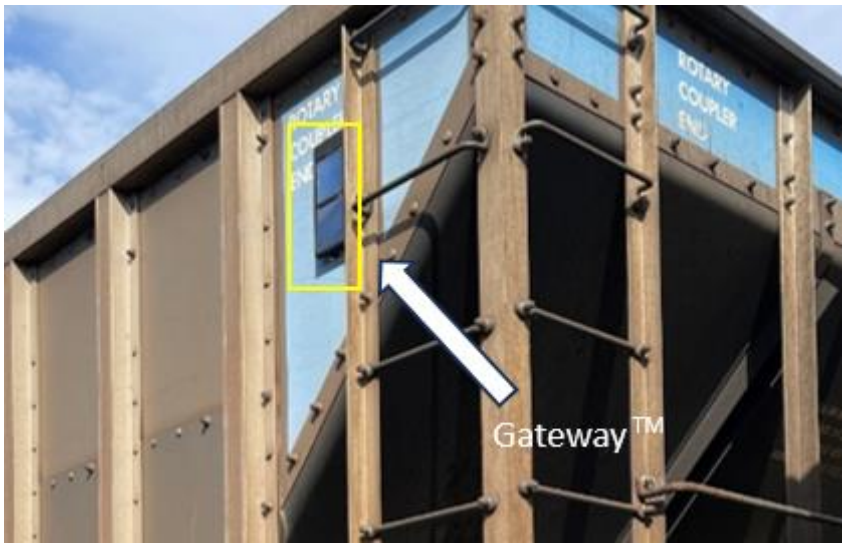

Figure 16: Gateway installation

CHAPTER III

BEARING AND WHEEL HEALTH INDICES

3.1 Bearing Health Index

The Bearing Health Index (BHI) is a nondimensional metric that is intended to characterize the condition of a bearing. The BHI functions similarly to the battery percentage indicator on a smartphone where the BHI decreases as the bearing condition deteriorates. It is based on the measured RMS (root-mean-square) values of the vibrational acceleration (G_{RMS}) generated by the bearing. It is intended to provide bearing diagnostics and prognostics to railroad operators in order to facilitate timely maintenance. This chapter presents the statistical analyses performed to develop the BHI.

3.1.1 BHI Correlation Development

The BHI model is a function of the measured G_{RMS} of a bearing operating at 100% of the AAR rated load and a train operating speed of 136.8 km/h (85 mph). These operating conditions were chosen to match the ones used when establishing the diagnostic and prognostic models. When making those models, there was an emphasis on expediting the results, and as such, the conditions that would lead to bearing failure the quickest, being the highest allowable loading condition and speed, were chosen. Moreover, these operating conditions allowed for worst-case scenario data sets to be collected. The vibration acceleration values used to produce the correlation are presented in Table 3.

Table 3: Vibrational acceleration values and their corresponding BHI values

Acceleration (G_{RMS})	BHI
4	10
8	7
12	5
15	3
25	1

The values selected for model development were based on statistical analysis of two decades' worth of bearing vibration data. Specifically, the first two values are based on the speed-dependent thresholds developed and optimized by the UTCRS. The preliminary threshold (at 85 mph) corresponds to a 4 G_{RMS} acceleration. Bearings that exhibit vibration levels that are at or below this threshold are considered healthy (defect-free). Therefore, any measured values at or below this value correspond to a BHI of 10, indicating that the bearing is at full health. The maximum threshold (at 85 mph) corresponds to an 8 G_{RMS} acceleration, where bearings that exhibit vibration levels above this threshold are deemed defective. However, bearing vibration levels falling between the two thresholds introduce uncertainty in determining whether the bearing is healthy but running at elevated vibration levels or contains a defect in its early stages of development. Thus, the range between these two thresholds (4 G_{RMS} - 8 G_{RMS}) has been designated the "gray zone" and corresponds to BHI values between 10 and 7. The latter acceleration values in Table 3 were chosen based on extensive research in defect propagation patterns through testing performed at the UTCRS and correspond to defect sizes based on correlations developed by Montalvo [21]. Figure 17 displays the exponential model generated utilizing the values in Table 3.

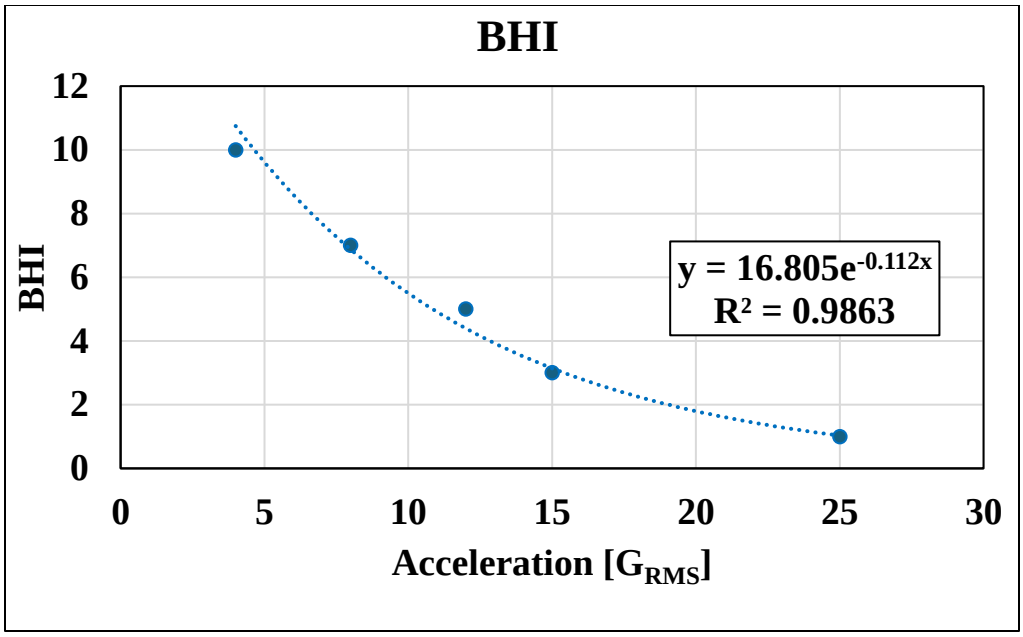

Figure 17: BHI correlation

3.1.2 BHI Normalization

The BHI correlation was developed with vibration data collected from fully loaded bearings operating at 136.8 km/h (85 mph). However, these conditions are uncommon in freight rolling stock and train speeds can vary significantly. Therefore, in order for the BHI to reflect bearing condition independent of speed, the measured vibration levels must be normalized. This process is done by converting the acceleration measured at the actual speed to the acceleration that would be expected at 136.8 km/h (85 mph). Correlations were developed using data from experiments with defective bearings running at speeds ranging from 40.2-136.8 km/h (25-85 mph). Only experiments where the defect did not propagate during testing were considered as to not bias the model with the effects of spall propagation. Figure 18 provides an example of a correlation relating the acceleration at 72.4 km/h (45 mph) to the acceleration at 136.8 km/h (85 mph). Similar correlations have been developed for the other operating speeds.

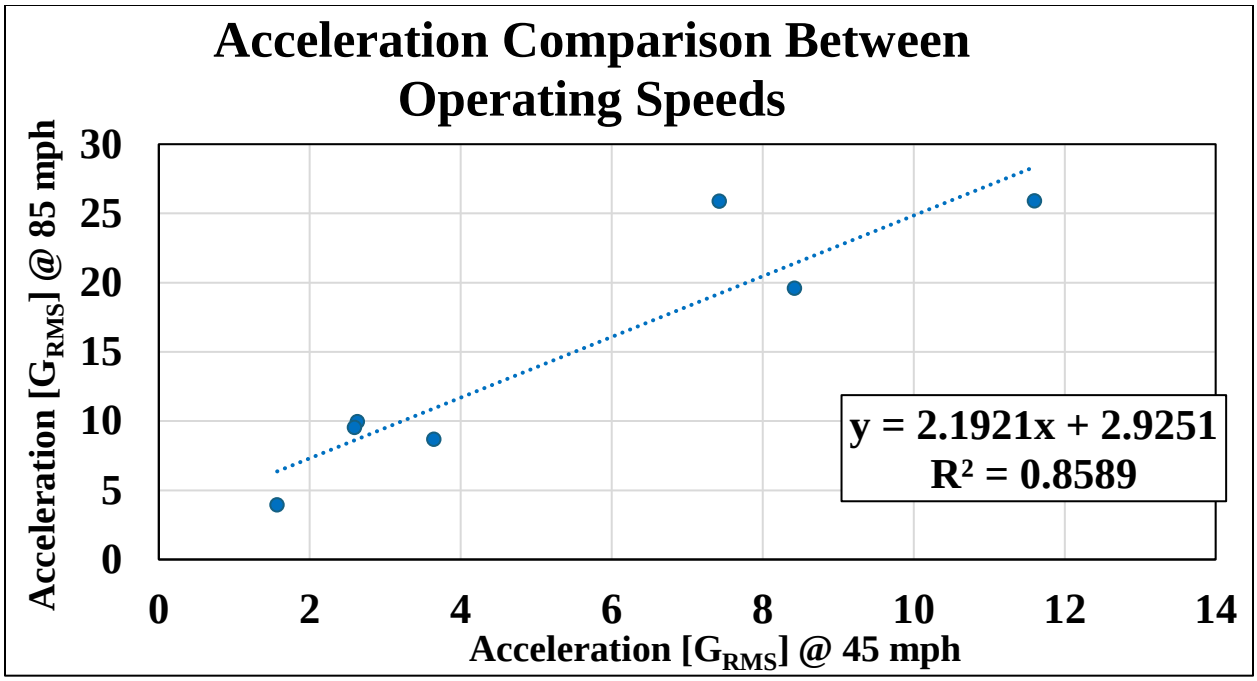

Figure 18: Correlation relating the acceleration values at 45 mph to those at 85 mph

It should be noted that these normalization correlations are still in development and will be further optimized as more data becomes available.

3.1.3 Bearing Diagnostic and Prognostic Model Implementation

To provide railroad operators with bearing diagnostics and prognostics, the BHI was incorporated with previously established models. With these models, the BHI can be used to provide estimates for the approximate defect size and the remaining useful life (RUL), which can be used to schedule proactive maintenance. Note that a BHI value of 1 indicates a bearing nearing the end of its service life, and should be removed from service at the next possible chance. In the study done by Montalvo [21], correlations relating acceleration values at 136.8 km/h (85 mph) to spall area for outer and inner rings were optimized. In its current configuration, the Boomerang does not distinguish between outer and inner ring defects in order to conserve power. Therefore, only the outer ring model was considered since outer ring defects initiate and

propagate at faster rates than inner ring defects, providing a worst-case scenario [2]. Using the worst-case empirical models developed by Lima [2], which relate spall area to propagation rate, the RUL is estimated. Table 4 displays the BHI values with their corresponding estimated cup spall sizes and RUL.

Table 4: BHI and corresponding cup spall sizes and RUL

BHI	Spall Area [cm^2] / [in^2]	RUL [km]	RUL [mi]
10	-	≥400,000	≥250,000
7	7.85 / 1.22	~300,000	~186,000
5	14.58 / 2.26	~136,000	~85,000
3	20.42 / 3.17	~80,000	~50,000
1	48.73 / 7.55	0	0

3.2 Wheel Health Index

The Wheel Health Index (WHI) is a nondimensional metric that is intended to represent the condition of a railcar wheel. Like BHI, a value of 10 indicates a healthy wheel, while a value of 1 signifies a wheel in need of urgent remediation. The wheel impact forces calculated from the measurements of the Boomerang's A2 accelerometer are passed through a correlation developed by Barrera [23] to output WHI.

3.2.1 WHI Correlation Development

Table 5 presents the values used to develop the correlation relating impact force to WHI. These values are roughly based on the AAR WILD guidelines summarized in Table 2. An impact force of 267 kN (60 kips) falls below the AAR threshold for optional maintenance, and is therefore assigned a WHI of 10, indicating a wheel of minimal concern. The A2 accelerometer

can only measure a maximum impact force of 454 kN. Therefore, a force of 445 kN (100 kips) corresponds to a WHI value of 1, indicating a potentially dangerous wheel that should be replaced as the forces could potentially be even higher than what the accelerometer can capture. The intermediate force values were chosen to allow for a linear relationship between force and WHI. Figure 19 displays the correlation developed with these values.

Table 5: Impact force values and their corresponding WHI values

Impact Force [kN]	Impact Force [kip]	WHI
267	60	10
311	70	7
356	80	5
400	90	3
445	100	1

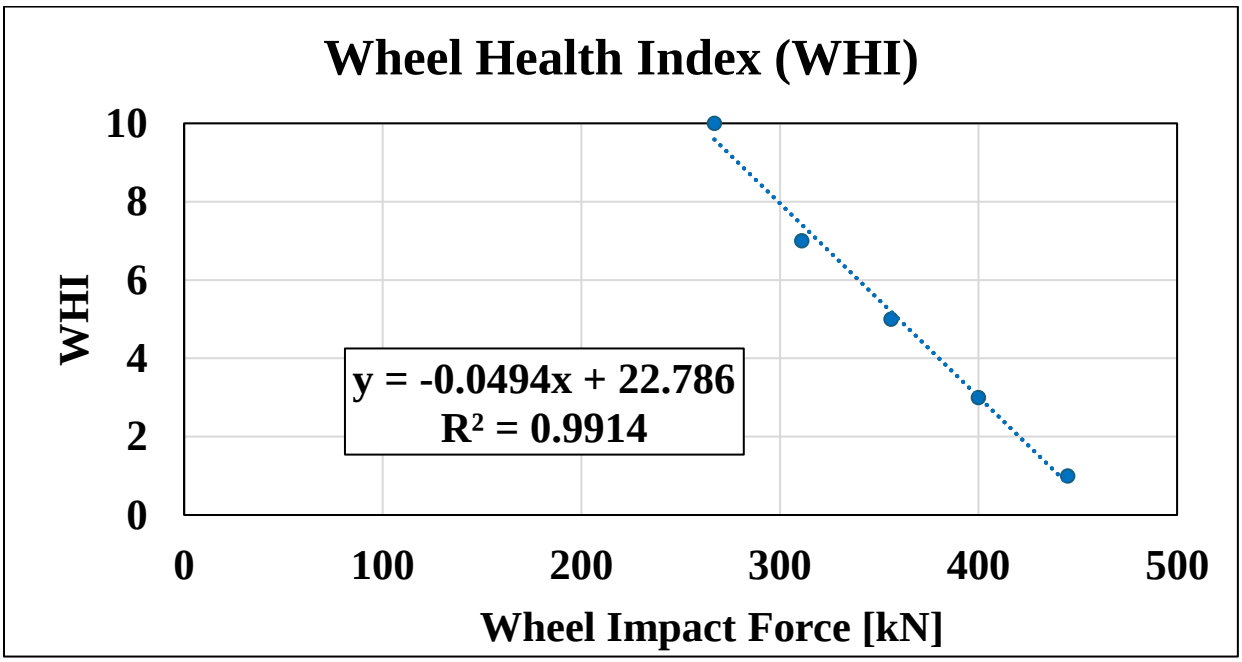

Figure 19: WHI correlation

CHAPTER IV

ACCOUNTING FOR VARIABILITY

This chapter aims to summarize the methods used to account for the variability in the vibration data taken from the field. Potential sources of variability include loading condition, track-related transients, defect propagation, and defect position. Any algorithm intended for accurate and reliable diagnostics and prognostics should be able to account for these variations and provide reasonable estimates.

4.1 Load-Induced Variability

Previous experimentation has shown that vibration signatures of defect-free bearings vary minimally with loading condition [19]. However, the same is not true for defective bearings. Increased loading results in an increased contact area between the roller and raceway. If the raceway contains a spall, the roller impacts the spall with a higher force, leading to elevated vibration levels. Figure 20 plots the laboratory acceleration as a function of speed of a bearing with a cup defect at unloaded (17%) and loaded (100%) conditions. It is evident that the vibration levels at each loading condition differ substantially as speed increases. Therefore, it is imperative to account for the load to characterize the condition of a bearing.

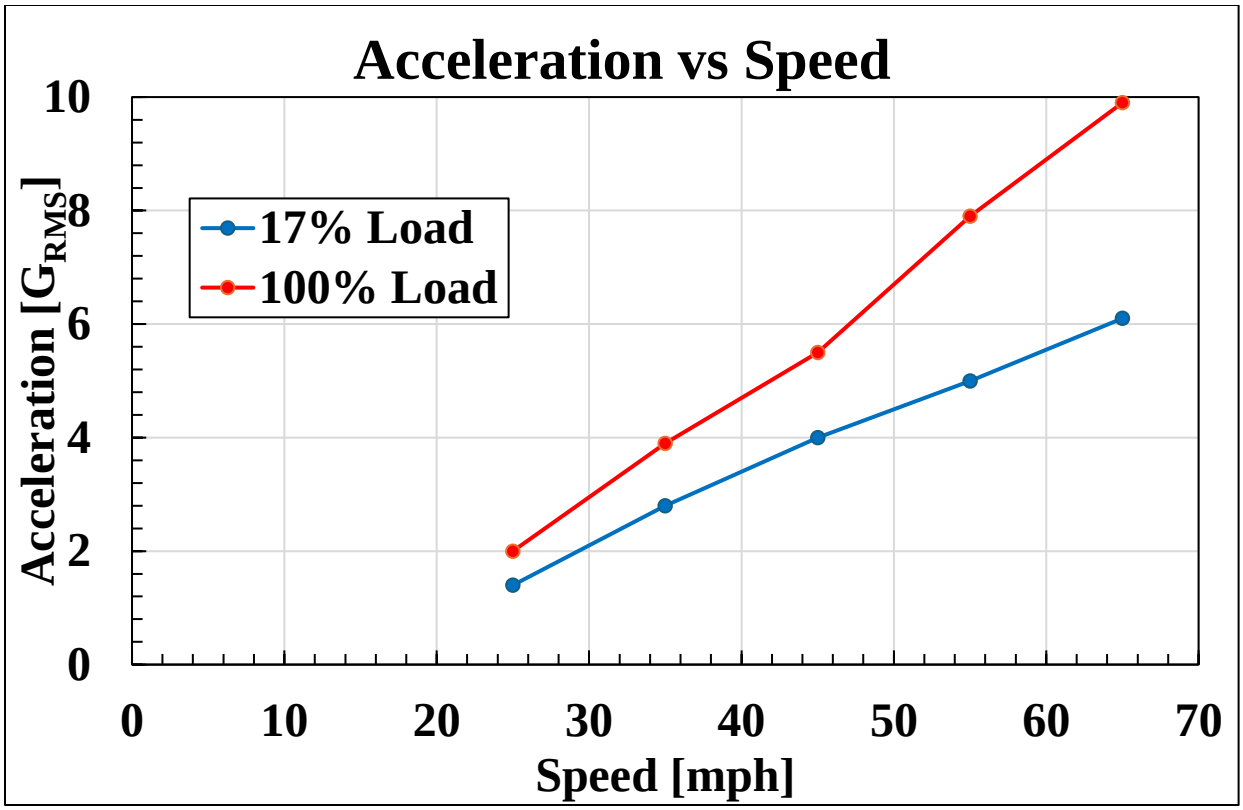

Figure 20: Acceleration vs speed for a bearing with a cup defect (31.2 cm^2)

The Hum condition monitoring system is able to determine loading condition based on the direction of travel of the railcar (utilizing GPS) and knowledge of the route it is undertaking. Currently, a load sensor is under research and development with the intention of integrating with the Boomerang/Gateway package to provide real-time loading conditions. As mentioned in Chapter III, the BHI is based on the normalized vibration level expected at 136.8 km/h (85 mph) and 100% load. Moreover, a study conducted by the FRA mentions that approximately 58% of railcar miles are travelled under load [24]. Therefore, the bearing diagnostic portion of the algorithm only considers data recorded under fully-loaded conditions, which is sufficient for the characterization of bearing health. More experimentation at unloaded conditions can be conducted to develop the correlations necessary to incorporate unloaded data in bearing diagnostics.

4.2 Track-Induced Variability

The data used to develop the BHI-based models was generated from laboratory experiments that do not simulate track conditions. The dynamics of wheel-track interactions can vary significantly due to track defects, grade-crossings, etc. These interactions can have a measurable effect on the vibration response captured by the Boomerang's accelerometers and result in outliers that are not representative of bearing or wheel condition.

The first method for removing these outliers is based on statistical analysis of the data captured by the A2 accelerometer, which is more sensitive to high-energy impacts. Outliers are identified and removed by grouping the data by train speed and excluding values that fall outside acceptable limits beyond the interquartile range at each speed. To further refine the data for BHI purposes, the Crest Factor, which is the ratio of the maximum G acceleration of the vibration signal over the G_{RMS} of the signal, calculated from A1 accelerometer data, was analyzed. Laboratory testing of healthy and defective bearings shows that the A1 Crest Factor never exceeds a value of 10. In contrast, simulated impact testing with healthy and defective bearings consistently produces Crest values above 10. Hence, a Crest value of 10 was established as a threshold for identifying high-energy track or wheel related impacts. Data points with tabulated Crest values exceeding 10 are excluded from BHI calculation.

4.3 Defect-Induced Variability

4.3.1 Vibration Patterns of Defect Propagation

Bearing defects do not produce predictable vibration profiles with respect to time. The vibration levels measured from a defective bearing can fluctuate randomly as the defect propagates and debris circulates within the raceways and is ground down by the rotation of the

rollers. Figure 21 provides an example of laboratory vibration data taken from a bearing that initiated a cup defect that propagated throughout the duration of the experiment. Note that the vibration levels rose above the maximum threshold (red line) indicating a defective bearing and eventually settled below it. As the BHI is based on the measured vibration levels, the BHI would increase as the vibration decreased, leading to a false indication of bearing health improvement. Thus, the algorithm retains the lowest BHI if the subsequent vibration data results in a higher BHI. Figure 22 compares the BHI and vibration profiles of the bearing from Figure 21. Note that the BHI does not improve even if the vibration levels decrease, which represents a more realistic depiction of bearing health, i.e., once the bearing develops a defect, it cannot heal itself.

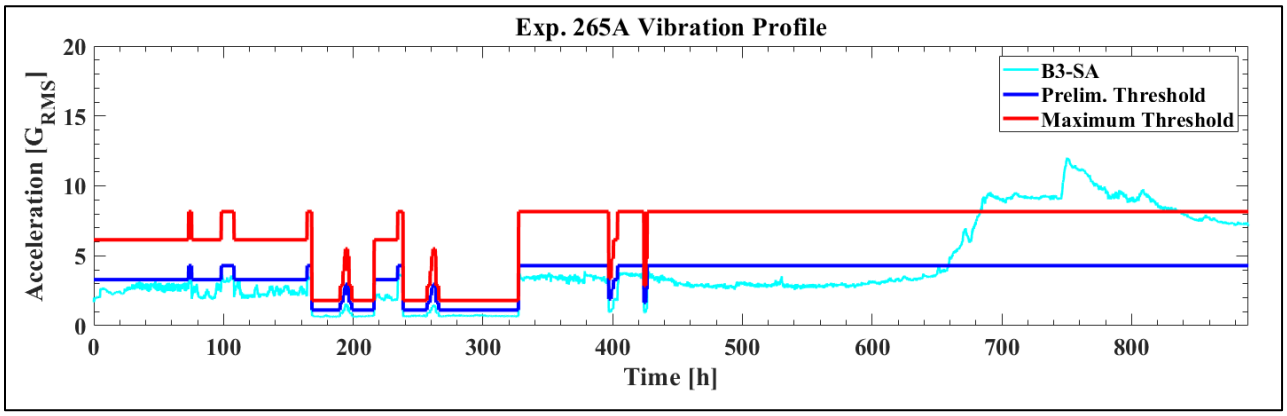

Figure 21: Vibration profile of a bearing that initiated a cup defect

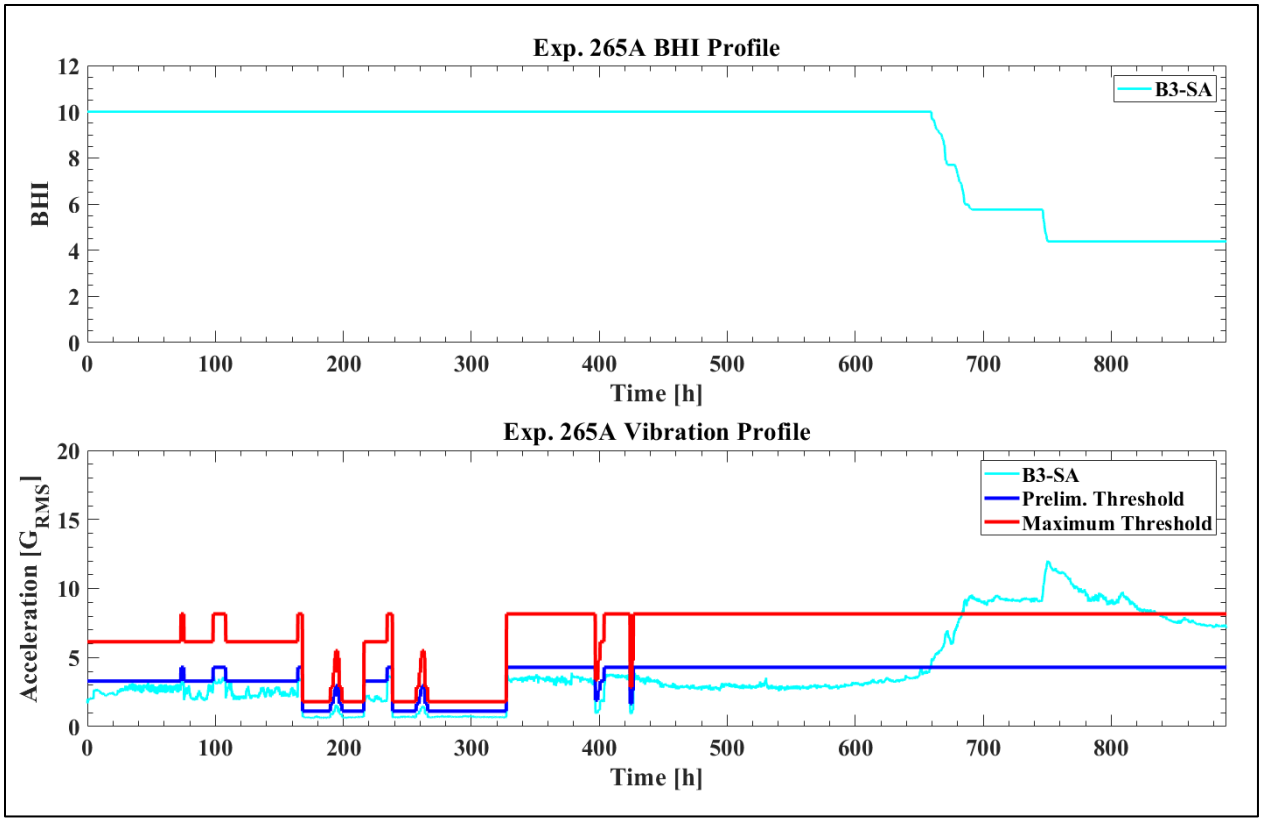

Figure 22: BHI and vibration profiles of bearing that initiated a cup defect

The final BHI calculated for this bearing was 4.38, which translates to an estimated spall size of 14.59 cm^2 (2.26 in^2). However, the actual size of the spall (seen in Figure 23) was measured to be 7.03 cm^2 (1.09 in^2), resulting in an error of 108%. This error in defect size estimation is likely due to three reasons. The first reason has to do with the spall measurement process, which only accounts for the main spall area and ignores the pitted regions that surround the spalled region. These pits can contribute to the vibration of the bearing, leading to an overestimation of the main spall area. The second reason is the inherent error in the normalization of the measured vibration values, and the third reason is that, in this particular example, the BHI was calculated using the highest normalized G_{RMS} value generated by the bearing. The issue with doing so is that the maximum G_{RMS} value may not be representative of

the true defect size. As defects develop and propagate, they produce debris (i.e. metal shards) that can temporarily generate higher levels of vibration that eventually settle as the debris is ground down by the rotating rollers.

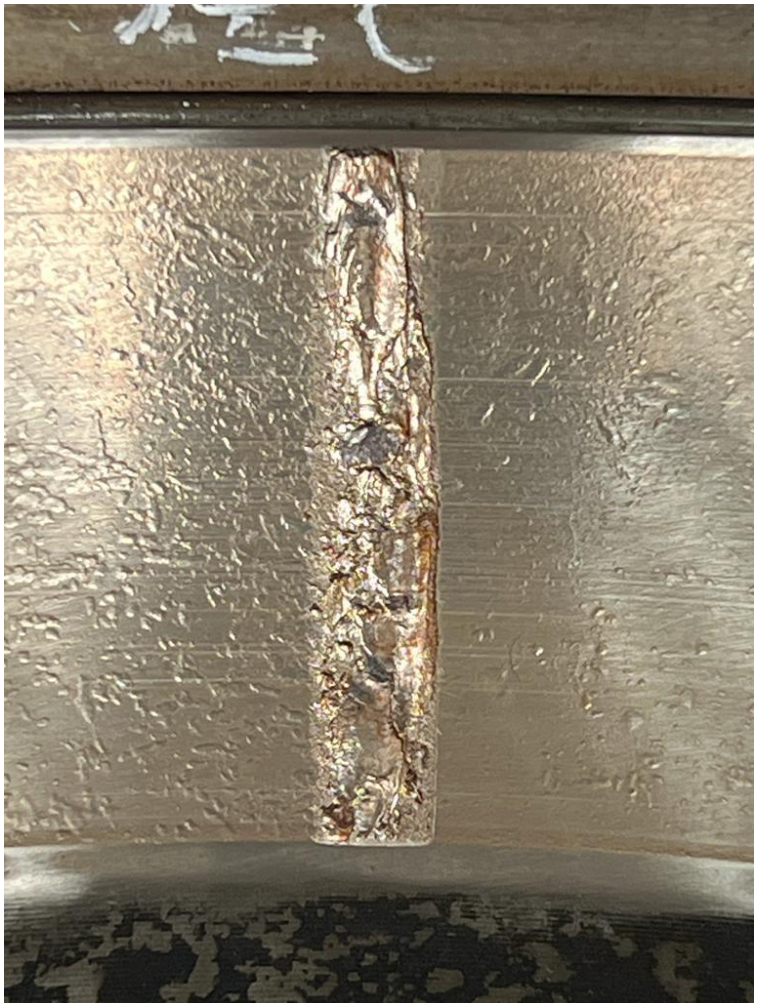

Figure 23: Cup spall initiated during Exp 265A

Figure 24 provides another example showcasing the vibration and BHI profiles of a bearing with a severe cup defect. The spall, pictured in Figure 25, was measured to be 62.58 cm^2 (9.70 in^2). The BHI was calculated to be 0.244 which translates to an estimated spall size of 95.57 cm^2 (14.81 in^2). This again resulted in an overestimation of the defect severity by 52.7%. The overestimation of the defect size necessitated a method to account for the variability

resulting from the normalized acceleration and defect propagation. In this particular example, if, instead of using the highest normalized acceleration, the average of the normalized G_{RMS} acceleration values was used to calculate the BHI, then the resulting BHI would be 0.762. This BHI value translates to an estimated spall size of 60.72 cm^2 (9.41 in^2), a difference of only 3% from the actual measured defect size, which represents a significant improvement in the accuracy of the BHI's diagnostic capability. Thus, for field service applications, the condition monitoring algorithm will be set to take the average normalized G_{RMS} from a day's worth of vibration data to calculate the BHI that best characterizes the bearing condition.

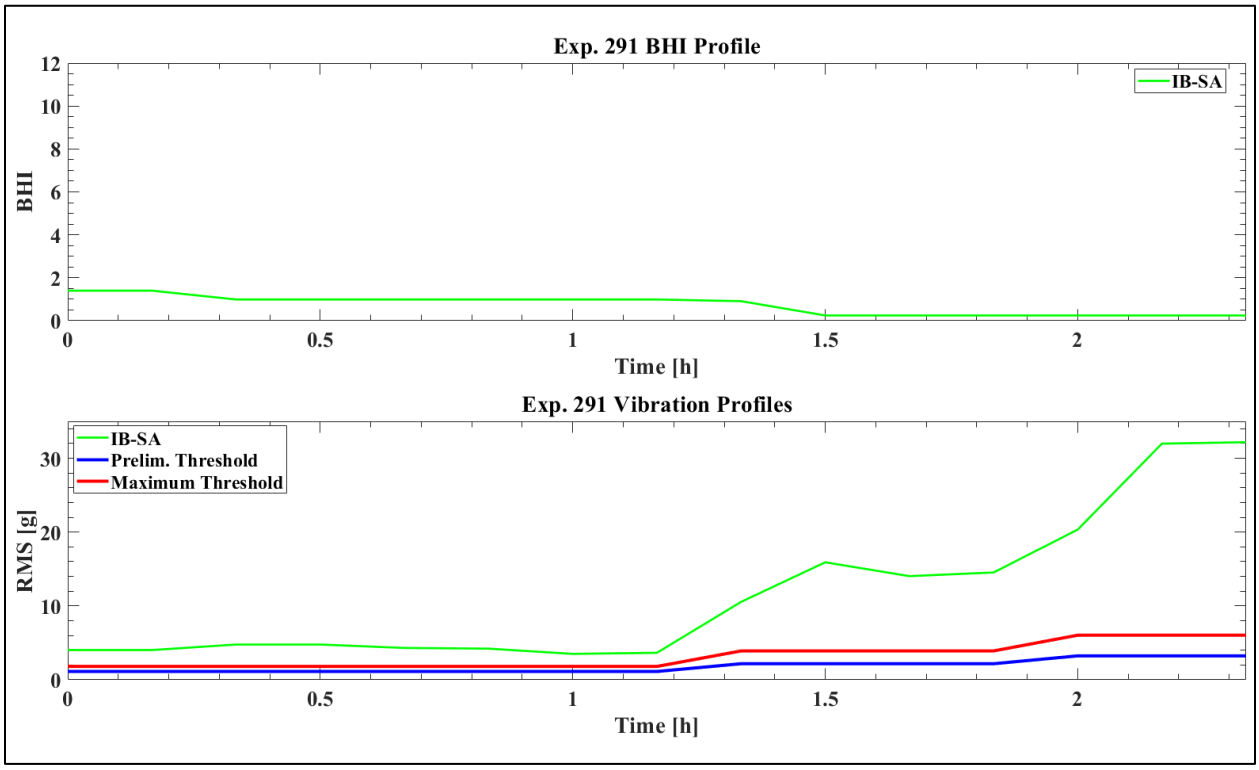

Figure 24: BHI and vibration profiles from a bearing with a severely defective cup raceway

Figure 25: Cup spall from Exp 291

4.3.2 Defect Location

The cup defect data used to develop the algorithm's models were collected with the defect positioned at top dead center within the raceway loaded zone, near the accelerometer. However, bearing cups, although intended to be stationary, can slowly rotate under the adapter due to wear, impacts, severe raceway defects, sudden braking, etc. This phenomenon is known as cup indexing. The vibration signatures of a bearing containing a defect on the cup raceway may vary over time as the cup indexes. This prompted an investigation into the effects of cup indexing on measured vibration profiles from bearings with cup defects. An experiment was performed on the UTCRS Single-Bearing Tester (SBT) to study this indexing behavior.

The cup used in this test contained a localized defect with an area of 23.9 cm^2 (3.70 in^2), pictured in Figure 26. The defect was placed at positions of 0° (top-dead-center, i.e., location of maximum applied load), 90°, 180°, and 270° with respect to the instrumentation location. The 0°

position was run a second time (denoted as 360°) to validate that the spall did not propagate throughout testing. Iterations for all defect positions were conducted with operating speeds of 40.2 km/h (25 mph), 72.4 km/h (45 mph), and 104.6 km/h (65 mph) under both unloaded and loaded conditions. Instrumentation included a V6 Boomerang, a wired version of A1 for reference, and another tri-axial accelerometer being tested as a possible replacement for the Boomerang's A1 accelerometer. Figure 27 depicts the mounting of the instrumentation to the adapter.

Figure 26: Cup spall used in index testing

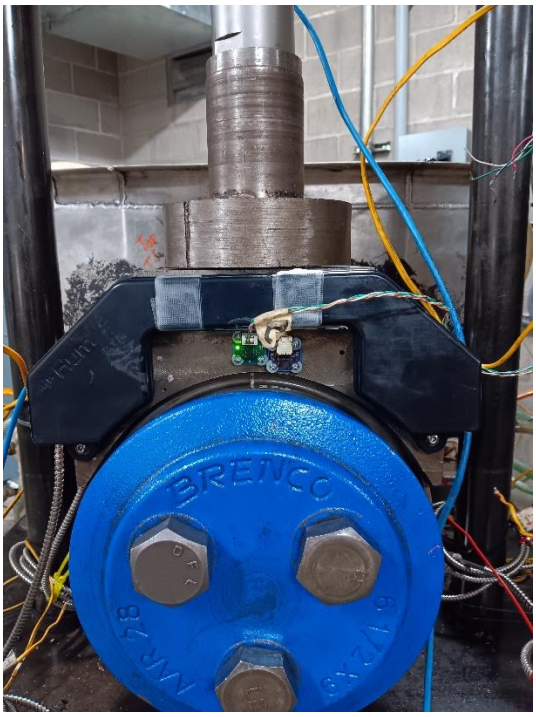

Figure 27: Instrumentation setup for index testing

Figure 28 and Figure 29 present the Boomerang A1 acceleration as a function of speed at all defect positions for unloaded and loaded conditions, respectively. The data shows that the position of the cup spall has a significant effect on the measured acceleration with higher values generally being measured with the defect directly under the instrumentation (i.e. 0° or top-dead-center, which also coincides with the region of maximum applied load). The 0° and 180° positions produced similar trends at unloaded conditions as they shared the same primary axis of vibration in the vertical direction. However, lower acceleration was recorded when the bearing was fully loaded with the defect at the 180° position as compared to the 0° position. This can be explained by the increased loading compressing the cup, leading the spall to move further away from the rollers. This increased separation between the spall and the rollers decreases the vibration levels as the rollers impact the defect with a lower force.

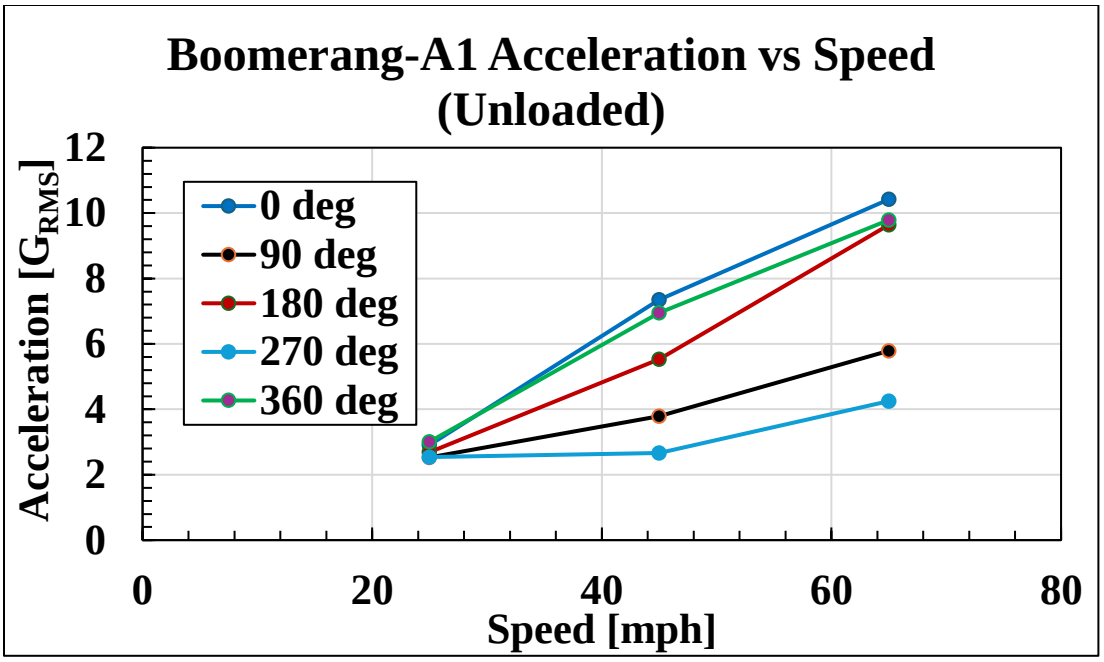

Figure 28: Boomerang A1 acceleration vs speed at unloaded conditions (all defect positions)

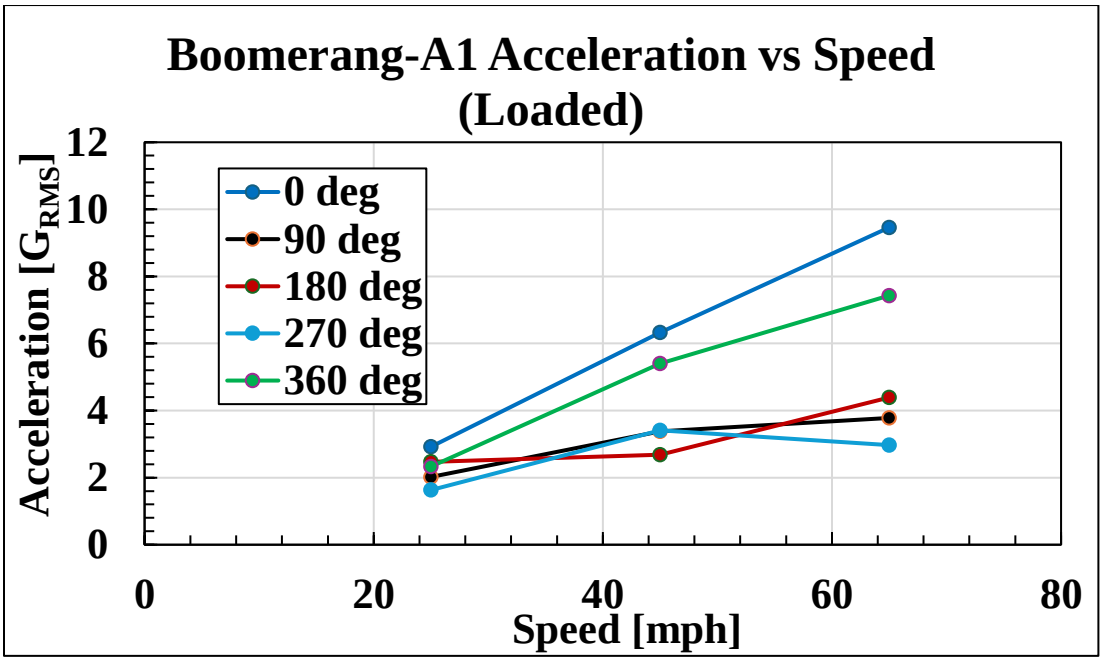

Figure 29: Boomerang A1 acceleration vs speed at loaded conditions (all defect positions)

Although it is evident that defect position has a measurable effect on bearing vibration levels, the algorithm can account for this utilizing the same method used to account for the propagation-induced variability. The algorithm retains the lowest BHI which corresponds to the highest measured acceleration value. Cup defects are most likely to initiate in the 0° position since this is the region that experiences the highest applied load. Therefore, even if the defect position shifts in the field due to indexing and the measured acceleration decreases, the algorithm will retain the lowest BHI calculated when the defect was located at top-dead-center. Moreover, if the defect propagates during indexing, then upon completing a full rotation, the acceleration values at the 0° position will be higher than in the previous cycle, resulting in a lower tabulated BHI. Thus, the algorithm can still provide reliable and accurate bearing diagnostics and prognostics even if the cup containing the spall (defect) indexes.

CHAPTER V

FIELD CONDITION MONITORING ALGORITHM

This chapter details the comprehensive field condition monitoring algorithm (FCMA) as it is currently being implemented on data received from Boomerangs in rail revenue service. The subsequent sections provide details of each step in the algorithm.

5.1 Step 1: Is the Wheelset Defective?

The first step of the algorithm is to determine whether the wheelset (also referred to as axle) assembly (consisting of the wheels, bearings, and axle) is defective. This is accomplished by analyzing the maximum acceleration data from the A2 accelerometer. The field test conducted by Barrera showed that the maximum acceleration measured by A2 of a healthy wheelset generally remains below a threshold of 20 g apart from a few outliers (likely track-related) [23]. Figure 30 presents the A2 data recorded from a newly installed, healthy wheelset on the railcar. From this data, it can be inferred that wheelsets with no defective bearings or wheels will generally exhibit acceleration values below the 20 g threshold. Therefore, to identify defective wheelsets, the algorithm applies the statistical filtering method described in Chapter IV to remove potential outliers, then calculates the percentage of data points that fall below the defined threshold. If less than 95% of the data is below the 20 g threshold, the algorithm flags that wheelset as most likely being defective and proceeds to the next step.

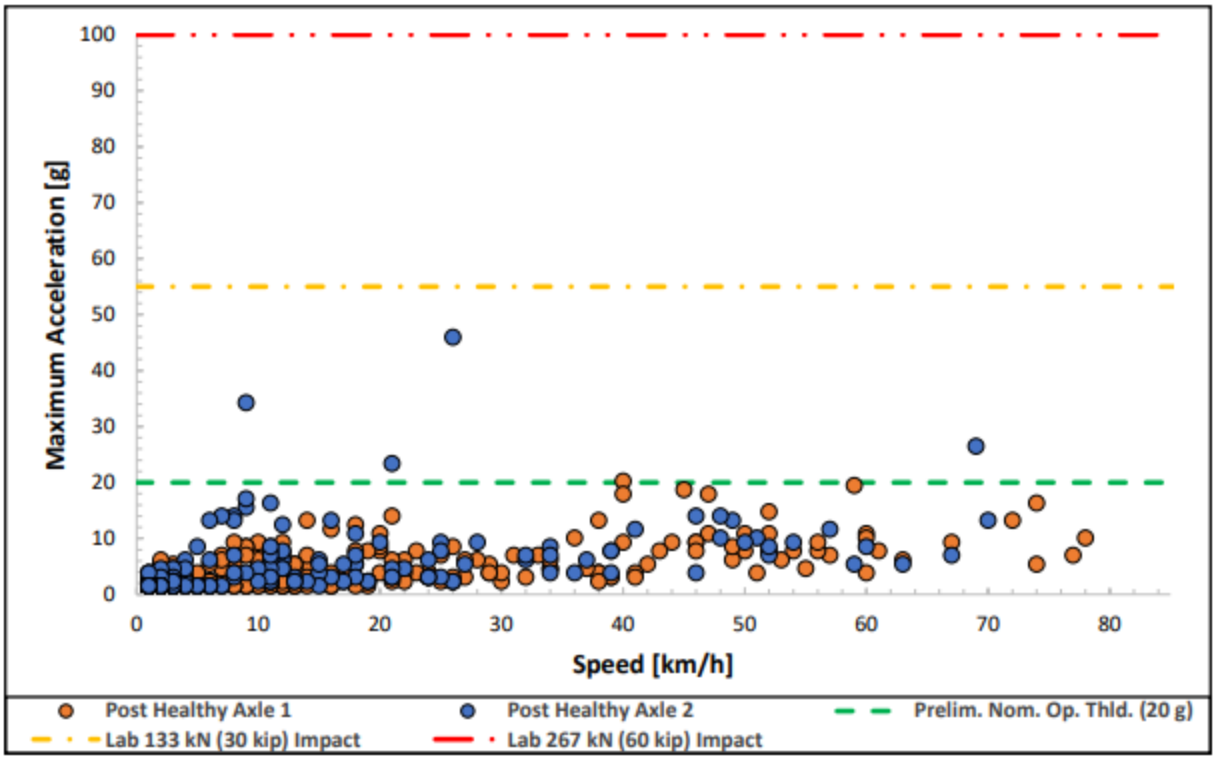

Figure 30: A2 acceleration data taken from a healthy wheelset [23]

5.2 Step 2: Bearing vs Wheel

Once a defective wheelset has been identified, the next step is to determine whether the bearing or wheel is defective. This step is challenging as both of the Boomerang's accelerometers are capable of detecting vibration signatures characteristic of either component being defective. Hence, this process requires an in-depth analysis of historical data to identify patterns indicative of a defective bearing or wheel. As mentioned in Chapter IV, the Crest Factor is a good indicator of the presence of impacts. Analysis of Crest data as a function of train speed for two defective wheels identified in a field test revealed a pattern that could aid the algorithm in identifying defective wheels. Figure 31 and Figure 32 display the A1 Crest data as a function of speed for both defective wheels denoted as W1 and W2, respectively.

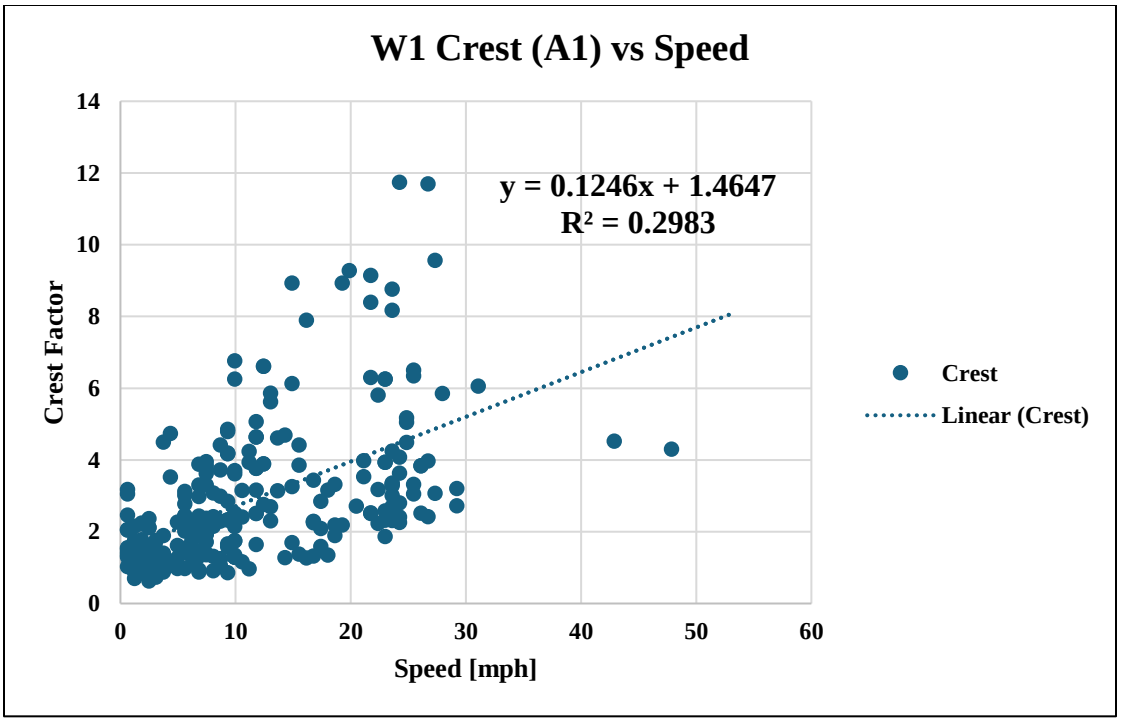

Figure 31: A1 accelerometer Crest vs speed for defective wheel W1 from field test

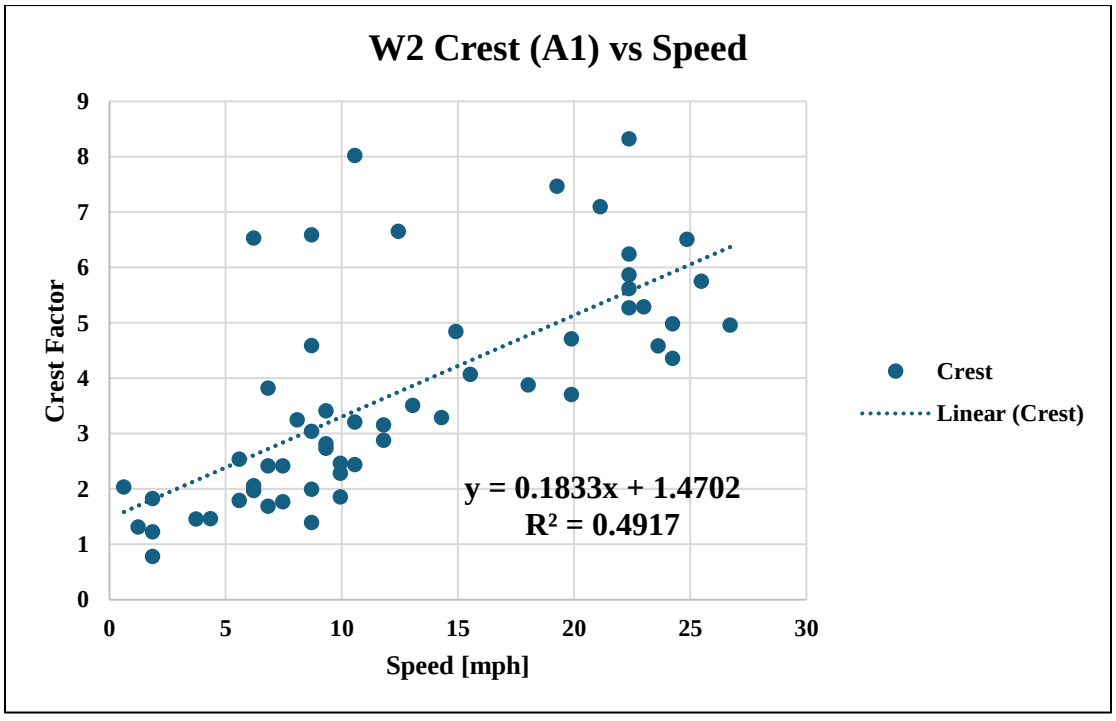

Figure 32: A1 accelerometer Crest vs speed for defective wheel W2 from field test

Linear regression analysis of the Crest data from the defective wheels reveals that the Crest tends to increase as a function of speed, indicating that higher speeds result in higher impact forces, which is expected. It should be noted that the majority of the data did not exceed the previously mentioned Crest threshold of 10. This is likely due to the impacts at lower speeds not generating enough force to push the Crest above the threshold. However, as the trendlines indicate, the Crest values would have crossed the threshold if the speed were to increase. Nonetheless, it is clear that defective wheels create a noticeable pattern in the Crest data. In contrast, laboratory experiments with defective bearings show that the Crest Factor is not influenced by operating speed. Figure 33 displays the vibration levels and Crest as a function of simulated distance travelled for two defective bearings running on the four-bearing test rig housed within the environmental chamber. The changes in the maximum threshold (red line) correspond to changes in operating speed. Note that the Crest values remain generally constant despite the presence of defects and changes in speed. Further analysis of five other experiments with defective bearings reveal similar patterns. Thus, analyzing Crest data as a function of speed can aid in the differentiation between defective bearings and wheels.

Currently, to determine if a wheelset has a defective wheel or bearing, the algorithm performs a linear regression analysis of the Crest from A1 as a function of speed. Two criteria must be met in order for the algorithm to designate the defective component as a wheel. First, the slope of the trendline must be at least 0.1 as the lowest slope value calculated from the field test was 0.125. Second, the correlation coefficient must have a value of at least 0.1 as the lowest value seen in the field test was 0.298. These values allow for some uncertainty as it is possible that less defective wheels could produce values below the ones seen in the field test. Note that

this is preliminary work based on limited data, and further field testing is needed to validate and analyze the Crest patterns for a wide variety of defect severities.

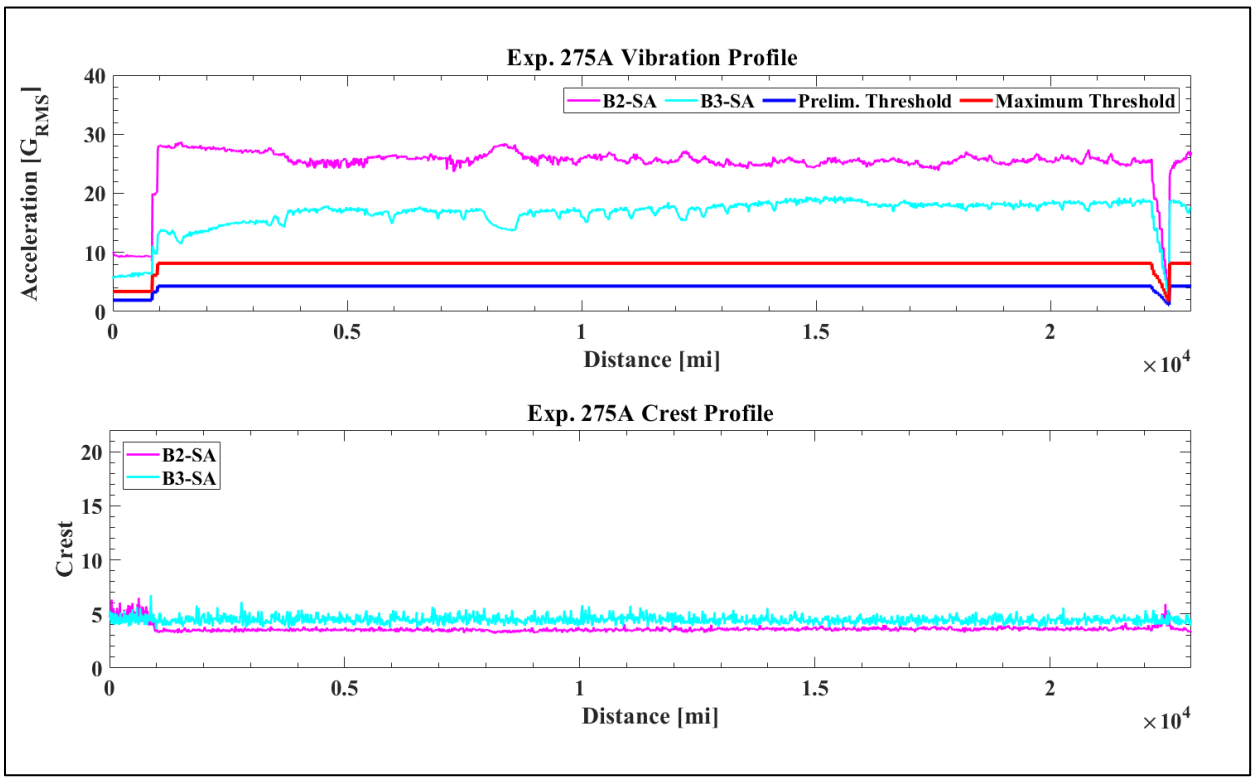

Figure 33: Laboratory vibration and crest profiles for two defective bearings

5.3 Step 3: How Defective is the Component?

Once the algorithm identifies whether a bearing or wheel is defective on a wheelset, it moves to the next step which is to determine how severe the defect is by calculating the BHI or WHI. For bearings, it does this by calculating the daily BHI from the daily average normalized G_{RMS} acceleration values. As mentioned in Chapter IV, the lowest BHI is retained to account for variability. For wheels, the algorithm determines defect severity by calculating the daily WHI from the daily maximum impact force. As with the BHI, the lowest WHI is retained. The BHI values calculated provide an estimate of the defect size and subsequently an estimate of the

remaining useful mileage. The WHI provides an indication of the severity of the impact loads generated by the wheel-rail interactions but cannot estimate the defect size or remaining mileage as these models have yet to be developed due to limited sample size and field testing.

CHAPTER VI

ALGORITHM EVALUATION

6.1 Laboratory Evaluation

This section aims to evaluate the performance of the FCMA in a laboratory setting. The Boomerang data used for this evaluation was taken from a bearing with a cup defect on the SBT. The cup (pictured in Figure 26) and instrumentation used in this experiment were the same ones employed in the indexing tests described in Chapter IV. The bearing was operated at speeds of 40.2 km/h (25 mph), 72.4 km/h (45 mph), and 104.6 km/h (65 mph) under both unloaded and loaded conditions.

6.1.1 Step 1: Is the Wheelset Defective?

Figure 34 displays the unloaded and loaded maximum acceleration data from the Boomerang's A2 accelerometer. It can be seen that a significant amount of data is above the 20 g threshold. The algorithm calculated that 50.5% of the data was above the nominal wheelset threshold, thus designating the "wheelset" as being defective. This demonstrates that the algorithm is capable of identifying defective "wheelsets" in a laboratory setting.

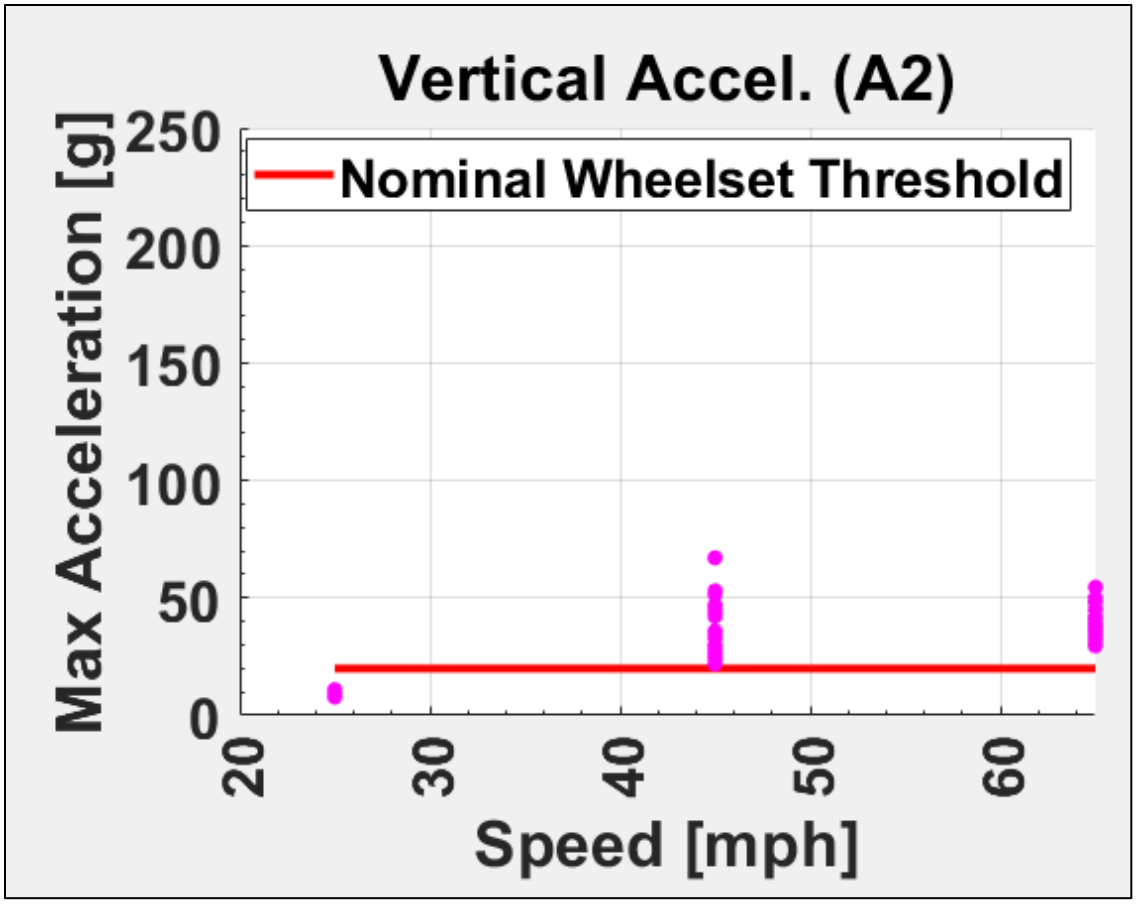

Figure 34: A2 accelerometer maximum g acceleration data as a function of speed (unloaded and fully loaded)

6.1.2 Step 2: Bearing vs Wheel

The next step of the algorithm is to determine the defective wheelset component through analysis of the A1 Crest data. Figure 35 shows the A1 Crest Factor as a function of operating speed. The algorithm calculated the correlation coefficient (R^2 value) and slope of the trendline to be 0.238 and 0.02, respectively. Although the correlation coefficient is above the 0.1 criterion established in Chapter VI, the slope of the line is below the 0.1 criterion resulting in the algorithm correctly identifying the bearing as being defective.

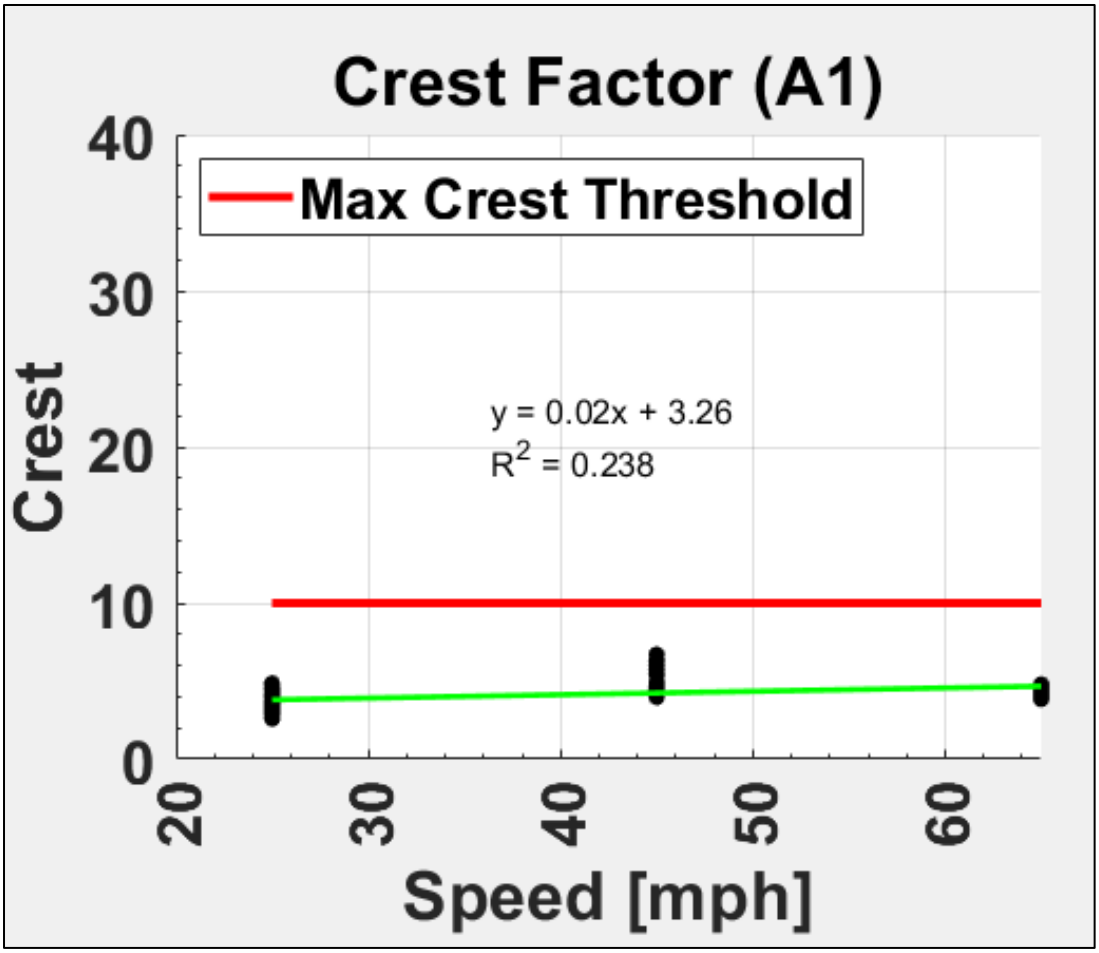

Figure 35: A1 accelerometer Crest Factor as a function of speed (unloaded and fully loaded)

6.1.3 Step 3: How Defective is the Component?

The algorithm calculated the average normalized acceleration to be 16.2 G_{RMS}, which translates to a BHI of 2.73. This corresponds to an approximate spall size of 23 cm^2 (3.57 in^2). Comparing these results to the actual measured spall size (23.9 cm^2 or 3.7 in^2) reveals that the algorithm was able to accurately determine the defect severity with a 3.8% difference. With this estimated size, the algorithm predicts an RUL of 64,797 km (40,262 mi) before the BHI reaches a value of 1, which is the threshold for recommending removal of the wheelset at the next

possible opportunity. This process provides railroad operators ample time to schedule proactive maintenance if this bearing were operating in rail revenue service.

6.2 Field Evaluation

This section evaluates the performance of the FCMA in a field setting. The data used for this evaluation was taken from Boomerangs installed on railcars during a field pilot test on a freight rail short line. From this test, a wheel was identified as being defective. Figure 36 displays the defects found on the tread of wheel R2.

Figure 36: Shelling on R2 wheel tread

6.2.1 Step 1: Is the Wheelset Defective?

Figure 37 presents the A2 accelerometer maximum acceleration data as a function of speed for wheel R2. It is visually evident that a considerable portion of the data is above the nominal wheelset threshold. The algorithm calculated that 55.4% of the data was above the threshold, thus correctly identifying that a component of the wheelset is defective.

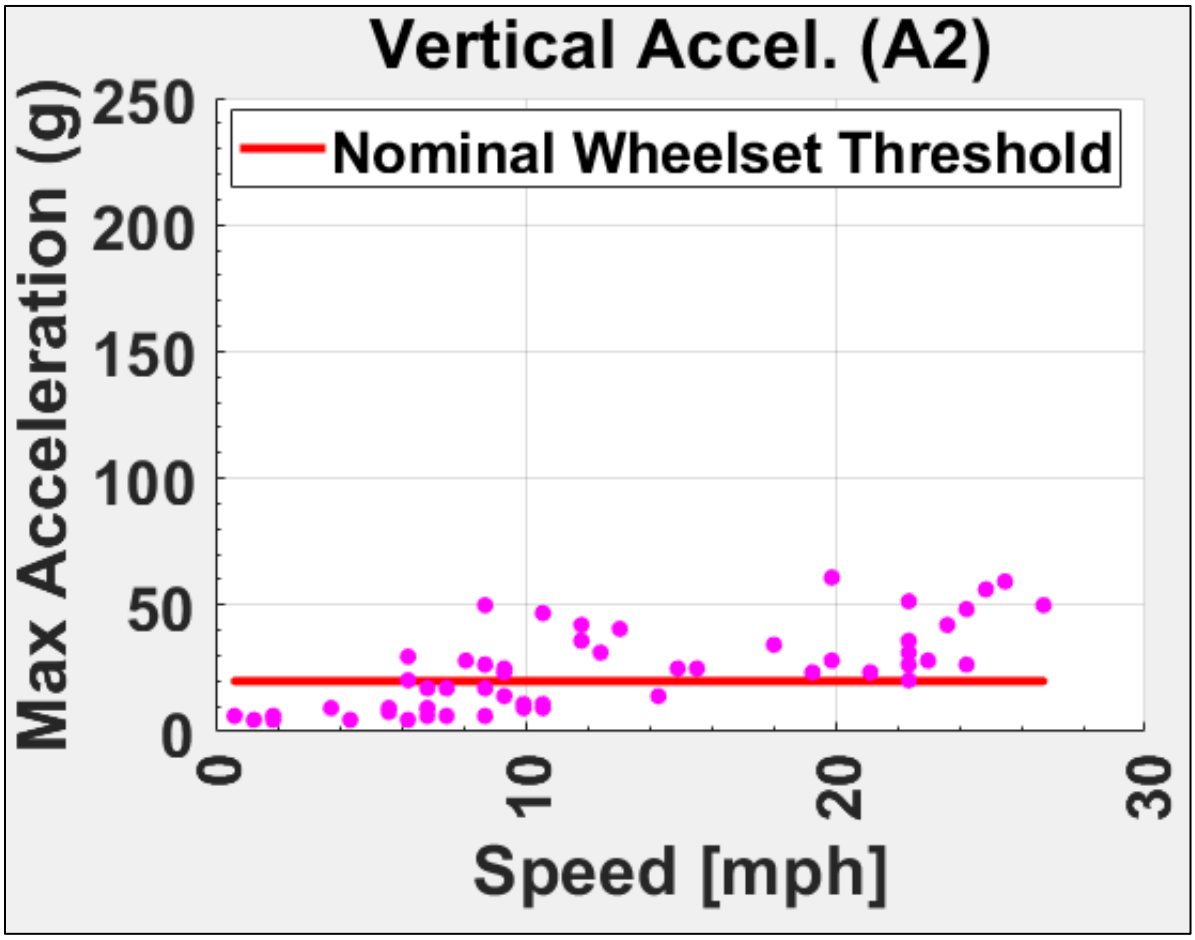

Figure 37: A2 accelerometer maximum acceleration data as a function of speed for wheel R2

6.2.2 Step 2: Bearing vs Wheel

Figure 38 shows the A1 Crest Factor as a function of speed for wheel R2. The R^2 correlation coefficient and slope of the trendline were calculated to be 0.492 and 0.18,

respectively, meeting both criteria needed to designate the wheel as defective. Therefore, the algorithm successfully identified the wheel as the defective component.

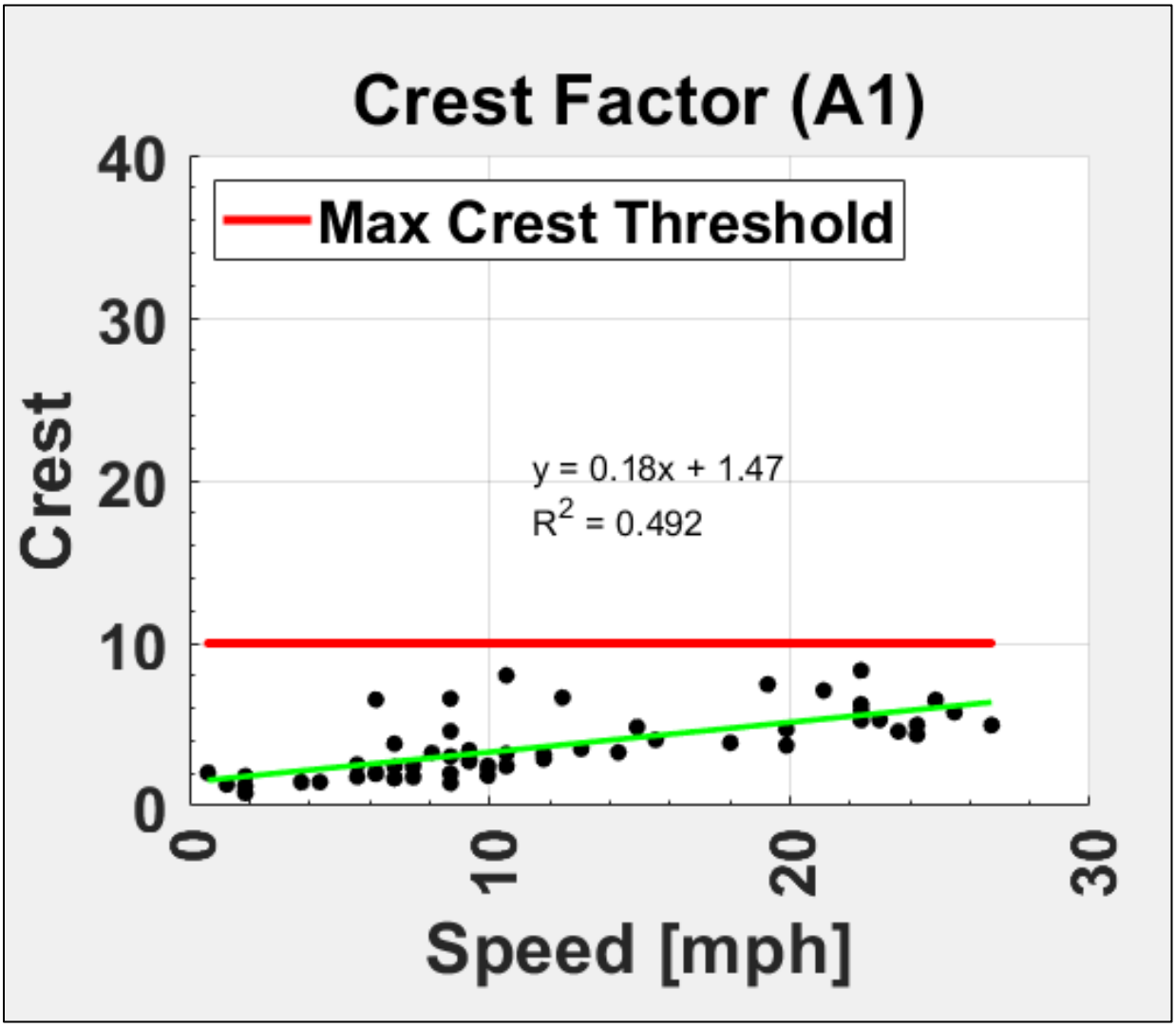

Figure 38: A1 Crest as a function of speed for wheel R2

6.2.3 Step 3: How Defective is the Component?

The highest wheel impact force recorded from wheel R2 was 133.45 kN (~30 kip). This corresponds to a WHI of 10, as it falls below the 267 kN (~60 kip) threshold, thereby classifying the wheel as healthy or of minimal concern. However, since the algorithm flagged the wheel as

defective and tread defects were confirmed upon inspection, a WHI of 10 does not necessarily indicate a defect-free condition. Thus, the algorithm is still able to identify defective wheels even if they do not produce impact forces that would be considered condemnable by AAR standards. Ultimately, this provides railroad operators with sufficient time to continue monitoring these wheels closely and schedule maintenance once they become problematic.

CHAPTER VII

CONCLUSIONS AND FUTURE WORK

The work presented in this thesis aimed to develop an algorithm designed to remediate the data-related challenges associated with onboard condition monitoring of freight rail bearings and wheels in rail revenue service and to provide reliable diagnostics and prognostics methodologies. These challenges included the differentiation between defective bearings and wheels, and the accurate characterization of component health despite the variability inherent in a noisy field environment. Data collected from over 200 laboratory experiments with healthy and defective bearings was utilized to generate models and provide a metric (i.e., Bearing Health Index - BHI) with diagnostic and prognostic capabilities for bearings. Data collected from laboratory testing with simulated impact loading aided in the construction of models used to produce a metric representative of wheel condition (i.e., Wheel Health Index - WHI). Field test data was utilized to identify patterns characteristic of defective wheels, which contributed to the distinction between defective bearings and wheels. Statistical and algorithmic methods were employed to account for variability from multiple sources and refine the accurate determination of bearing and wheel condition.

The condition monitoring capabilities of the field condition monitoring algorithm (FCMA) were successfully validated. The algorithm was able to reliably identify defective bearings in a laboratory setting. For the example provided in this thesis, which is representative of the testing done for this study, the FCMA was able to provide an accurate diagnostic of the

bearing defect, and estimate the spall size within 3.8% difference from the actual spall area. It estimated the RUL to be 64,797 km (40,262 mi), which gives railroad operators ample time to schedule proactive maintenance and mitigate unnecessary and costly train stoppages and delays. The algorithm was also successful in the early identification of a defective wheel operating in the field despite the low impact forces measured. Hence, proof of concept validation has been established. The algorithm, coupled with Hum's onboard condition monitoring system, can be an effective tool in providing railroad operators with diagnostics and prognostics that can aid in mitigating catastrophic train derailments.

7.1 Limitations and Future Work

To optimize power management, the current firmware of the condition monitoring system is set up to characterize the bearing condition. In order for the algorithm to distinguish between cup, cone, and roller defects in bearings, the complete data set collected must be transmitted wirelessly to the Gateway unit, which increases the power consumption of the Boomerang units. Therefore, only the cup diagnostic and prognostic models were implemented into the algorithm to represent a worst-case scenario. Inaccuracies with this model exist when estimating the RUL of bearings possessing either cone or roller defects. Despite this, the estimates provided by the cup models are conservative in nature and would likely overestimate the cone or roller defect severity, leading to enough advance notice for remediation of any problematic bearing. The correlations used to normalize the measured G_{RMS} values for speed were developed using a limited amount of data from experiments where the spall did not propagate throughout testing. Moreover, the majority of experiments used involved cup defects. More experimentation should be conducted with a wide variety of defect types and sizes to further refine the correlations.

With the current impact mechanism on the SBT, laboratory impact testing is not reflective of defective wheel dynamics in the field. The highest impact frequency used was 3 Hz (i.e., 3 hits per second) which simulates a wheel with a single defect travelling at 30.6 km/h (19 mph). This speed was used to mitigate fatigue failures in the impact mechanism components. Moreover, the impact force is fixed at a constant amplitude during testing regardless of the operating speed of the bearing. In field conditions, both the impact force and frequency are a function of speed. Thus, a redesign of the impact mechanism that can more accurately simulate these dynamics is needed to further map the response of the Hum system and algorithm to defective wheels in the field. The latter will contribute to the recognition of patterns that can aid in the identification of cases where both the wheel and bearing are defective.

REFERENCES

[1] N. De Los Santos, *Development of Prognostics Techniques for Surface Defect Growth in Railroad Bearing Rolling Elements*, Master's Thesis, Dept. of Mechanical Engineering, Univ. of Texas Rio Grande Valley, 2019.

[2] J. D. Lima, *Residual Service Life Prognostic Models for Tapered Roller Bearings*, Master's Thesis, Dept. of Mechanical Engineering, Univ. of Texas Rio Grande Valley, 2020.

[3] Desai, Rajiv. Train Wheel. October 28, 2017. [Online]. https://drrajivdesaimd.com/2017/10/28/derailment/comment-page-1/. [Accessed 15 January 2025].

[4] Indian Railways Institute of Mechanical and Electrical Engineering (IRIMEE), Wheel Defects & Wheel Shelling, Indian Railways, [Online]. Available: https://rskr.irimee.in/sites/default/files/WHEEL%20DEFECTS%20%26%20WHEEL%20SHELLING%28soft%20copy%20%29_0.pdf. [Accessed: May 8, 2025].

[5] U.S. Department of Transportation, *Train Accidents by Type and Rates*, Federal Railroad Administration Office of Safety, [Online]. Available: https://safetydata.fra.dot.gov/officeofsafety/publicsite/query/TrainAccidentsFYCYWithRates.aspx. [Accessed: Feb 4, 2025].

[6] S. Karunakaran, T.W. Snyder, 2007, "Bearing temperature performance in freight cars," Proceedings Bearing Research Symposium, sponsored by the AAR Research Program in conjunction with the ASME RTD Fall Conference, Chicago, IL, September 11- 12.

[7] Predikto. N.p.: Predikto, n.d. *Predicting Hot Box Detector Failures*. Predikto, 2015.

[8] Association of American Railroads, "Freight Railroads Announce Key Safety Measures in Drive to Zero Accidents," *Association of American Railroads*, Mar. 8, 2023. [Online]. Available: https://www.aar.org/news/freight-railroads-announce-key-safety-measures-in-drive-to-zero-accidents/. [Accessed: Feb. 4, 2025].

[9] Ose, Mixanikos. "Heat Detectors-box and Brake Disc (Hot Box & Hot Wheel Detection System)." Heat Detectors-box and Brake Disc (Hot Box & Hot Wheel Detection System). N.p., 16 July 2015. Web.

[10] C. Tarawneh, A. Martinez, M. Adame, S. Garcia, J. Pams, and C. Pena, "Healthy and Defective Tapered Roller Bearing Temperature Metrics," in *Proceedings of the 2024 Joint Rail Conference*, Columbia, SC, USA, May 2024, Paper No. JRC2024-128512. [Online]. Available: https://doi.org/10.1115/JRC2024-128512. [Accessed: Feb. 4, 2025].

[11] C. M. Tarawneh, L. Sotelo, A. A. Villarreal, N. de los Santos, R. L. Lechtenberg, and R. Jones, "Temperature profiles of railroad tapered roller bearings with defective inner and outer rings," in *Proc. ASME Joint Rail Conf. (JRC)*, Columbia, SC, USA, Apr. 2016, pp. V001T01A004. doi: 10.1115/JRC2016-5816.

[12] National Transportation Safety Board, *Norfolk Southern Railway Derailment and Hazardous Materials Release, East Palestine, Ohio, February 3, 2023*, Railroad Investigation Report RIR-24-05, June 25, 2024. [Online]. Available: https://www.ntsb.gov/investigations/AccidentReports/Reports/RIR2405%20CORRECTED.pdf. [Accessed: Feb. 4, 2025].

[13] Marketing, Nuthouse. "Advanced Rail Engineering." Etion Digitise, www.ansysrail.co.za/trackside-solutions/.

[14] B. Shannon, "DataTraks Secures Contract to Manage Trackside Acoustic Detection System (TADS)."DataTraks Secures Contract to Manage Trackside Acoustic Detection System (TADS). Builtin Colorado, 30 June 2014.

[15] "Trackside Acoustic Detection System." 2954TADS-03_2011.Cdr, Transportation Technology Center, Inc., Mar. 2011, www.aar.com/pdfs/TADS_OnePager.pdf.

[16] Stewart, M. F., Flynn, E., Marquis, B., Sharma & Associates. Department of Transportation. Federal Railroad Administration. An Implementation Guide for Wayside Detector Systems. Washington: GPO, 2019. Web. 10 Dec. 2020.

[17] S. Galván-Núñez, T. Sultana, and A. Poudel, *WILD Alerting on Empty Intermodal Carloads*, TD21-026, Assoc. of American Railroads (AAR)/MxV Rail, Sept. 2021. [Online]. Available: https://www.mxvrail.com/wp- content/uploads/2023/01/TD21-026.pdf. [Accessed: Feb. 4, 2025].

[18] Government of Canada, Transportation Safety Board of Canada. "Rail Transportation Safety Investigation Report R18W0007." Transportation Safety Board of Canada, / Transportation Safety Board of Canada, 5 Dec. 2019, https://www.bsttsb.gc.ca/eng/rapports-reports/rail/2018/r18w0007/r18w0007.html. [Accessed: Feb. 4, 2025].

[19] I. Alvarado, *Defect Detection in Railroad Tapered-Roller Bearings Using Vibration Analysis Techniques*, Master's Thesis, Dept. of Mechanical Engineering, Univ. of Texas Rio Grande Valley, 2012.

[20] A. Gonzalez, *Development, Optimization, and Implementation of a Vibration Based Defect Detection Algorithm for railroad Bearings*, Master's Thesis, Dept. of Mechanical Engineering, Univ. of Texas Rio Grande Valley, 2015.

[21] J. Montalvo, *Defect Detection Algorithm Optimization for Use in Freight Railcar Service*, Master's Thesis, Dept. of Mechanical Engineering, Univ. of Texas Rio Grande Valley, 2019.

[22] L. R. Cantu, *Assessing the Effectiveness and Efficacy of Wireless Onboard Condition Monitoring Modules in Identifying Defects in Railroad Rolling Stock*, Master's Thesis, Dept. of Mechanical Engineering, Univ. of Texas Rio Grande Valley, 2021.

[23] M. A. Barrera, *Railcar Wheel Impact Detection Utilizing Vibration-Based Wireless Onboard Condition Monitoring Modules*, Master's Thesis, Dept. of Mechanical Engineering, Univ. of Texas Rio Grande Valley, 2022.

[24] ICF International, "Comparative Evaluation of Rail and Truck Fuel Efficiency on Competitive Corridors," Federal Railroad Administration, U.S. Department of Transportation, Washington, D.C., Mar. 2009. [Online]. Available: https://railroads.dot.gov/sites/fra.dot.gov/files/fra_net/2925/Comparative_Evaluation_Rail_Truck_Fuel_Efficiency.pdf

VITA

Jeffery Ray Pams attended South Texas Business Education and Technology Academy and graduated in 2018. He received his Bachelor of Science in Mechanical Engineering from the University of Texas-Rio Grande Valley (UTRGV) in May 2023. He furthered his education at UTRGV and earned his Master of Science in Mechanical Engineering in May 2025. Jeffery conducted research in the rail transportation sector at the University Transportation Center for Railway Safety (UTCRS) from 2022-2025, specializing in condition monitoring of rolling stock. His achievements were recognized by the US Department of Transportation and received the UTC Student of the Year Award in 2025. He also received the Outstanding Graduate Student Award for academic achievement from the Department of Mechanical Engineering at UTRGV. Jeffery also commissioned as an officer in the Texas Army National Guard in May 2023 where he currently serves as an infantry Platoon Leader. He can be reached by email at jeffery.r.pams.mil@army.mil.